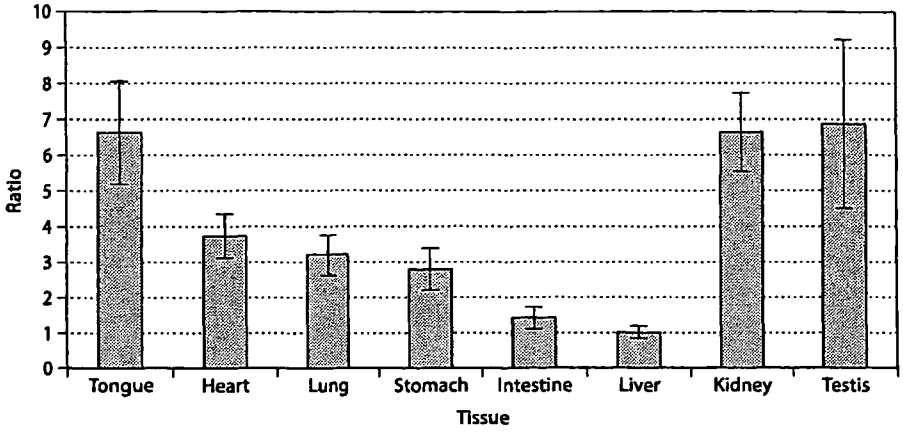

Fig. 6. Measurement of *TAS1R3* gene expressions in tissues by real-time PCR. RNA was prepared from tongue, heart, lung, stomach, intestine, liver, kidney, and testis, and subjected to real-time PCR as described in Materials and methods. Eight real-time measurements were made for each tissue sample, and mean values and standard errors were calculated for each sample. Values thus obtained were recalculated taking the mean value of liver as 1.0, and resulting values were plotted in this figure.

peptide (http://www.cbs.dtu.dk/services/SignalP/). The entire region of 33 consecutive amino-acids (i.e., 15 amino-acids plus the 18 amino-acid sequence corresponding to the signal peptide of the protein from Tonguel) at N-terminus of the protein from Tes2, was recognized as signal peptide. Therefore it is likely that TAS1R3 generated from Tes2 is functionally identical to those from the other transcripts.

DNA sequences of possible control region for TAS1R3

Since the 346 bp at the 5′ terminus of the 2,848-bp segment located upstream of the *TAS1R3* translation start site was indicated to be a part of a gene corresponding to human *MGC10334* or mouse *BC002216* (orthologue of human *MGC10334*) (http://www.ncbi.nlm.nih.gov/BLAST/) (see Fig. 3A), the sequence of the segment excluding the 346 bp was compared with the corresponding human and mouse sequences. The comparison indicated that the swine sequence from the translation start site to 317 bp upstream of the start site (designated as 317 bp sequence) showed a similarity to the corresponding human and mouse regions. The swine 317 bp sequence was then subjected to analysis of transcription factor binding sites (http://www.cbrc.jp/research/db/TFSEARCHJ.html), which revealed SRY and GATA-1/GATA-2 binding sites in the region (data not shown). The SRY binding site was also found in the corresponding human and mouse regions. When the swine sequence excluding the 317 bp and 346 bp sequences was subjected to the analysis of transcription factor binding sites using the above website, the analysis demonstrated 43 transcription factor binding sites, none of which, however, were commonly found in the corresponding human and mouse sequences (data not shown). These findings taken together indicated that the SRY binding site in the 317 bp sequence might function to control the transcription of *TAS1R3*.

Expression of TAS1R3 in swine tissues

The expression of *TAS1R3* in swine was investigated in tongue, heart, lung, stomach, intestine, liver, kidney, and testis by real-time PCR (Fig. 6), the results of which were normalized with reference to the amount of EGFP RNA added as a control along with the RNA samples. Tongue, kidney, and testis expressed the *TAS1R3* gene at a much higher rate than other tissues (Fig. 6). It was also demonstrated that heart, lung, and stomach expressed the gene significantly more than intestine and liver, though the extent of the elevations was small. The feature of *TAS1R3* gene expression in swine tissues examined was found to be essentially the same as that for mouse except that kidney expressed the gene as much as tongue in swine.

Determination of TAS1R3 gene expression sites in tissues

In order to investigate the localization of *TAS1R3* gene expression within various tissues, tongue, testis, and kidney were subjected to in situ hybridization using the RNA probes derived from exon 6. As shown in Fig. 7, tongue was found to express the gene in the circumvallate papillae (Fig. 7A), fungiform papillae (Fig. 7B), mucosal epithelium cells (Fig. 7A and 7B), lymphocytes in submucosal tissues of the lingual tonsil (Fig. 7C), and follicular B lymphocytes (Fig. 7D). Spermatogenic cells within the testis were also found to express the gene (Fig. 7E). Gene expression in kidney appeared uniform rather than specific to certain cells (data not shown). We have reached essentially the same in situ hybridization results using a different RNA probe from nt+137 to nt+317 (exon 1 and 2) (data not shown), providing supportive evidence for the findings obtained in the present study.

In order to confirm that swine B lymphocytes expressed *TAS1R3*, mature B lymphocytes were prepared from peripheral blood cells by a cell-sorter using an anti-CD21 antibody

Fig. 7. Expression of *TAS1R3* in swine tissues. Red and black arrows in **A** indicate tongue circumvallate papillae and mucosal epithelium, respectively; in **B**, they indicate tongue fungiform papillae and mucosal epithelium, respectively; (**C**) lymphocytes in submucosal tissue of lingual tonsil; (**D**) follicular B lymphocytes; and (**E**) spermatogenic cells in testis. (A1–E1) Results of in situ hybridization using RNA anti-sense probe (detection of *TAS1R3* sense message); (A2–E2) results of hybridization using RNA sense probe; and (A3–C3) staining with hematoxylin and eosin.

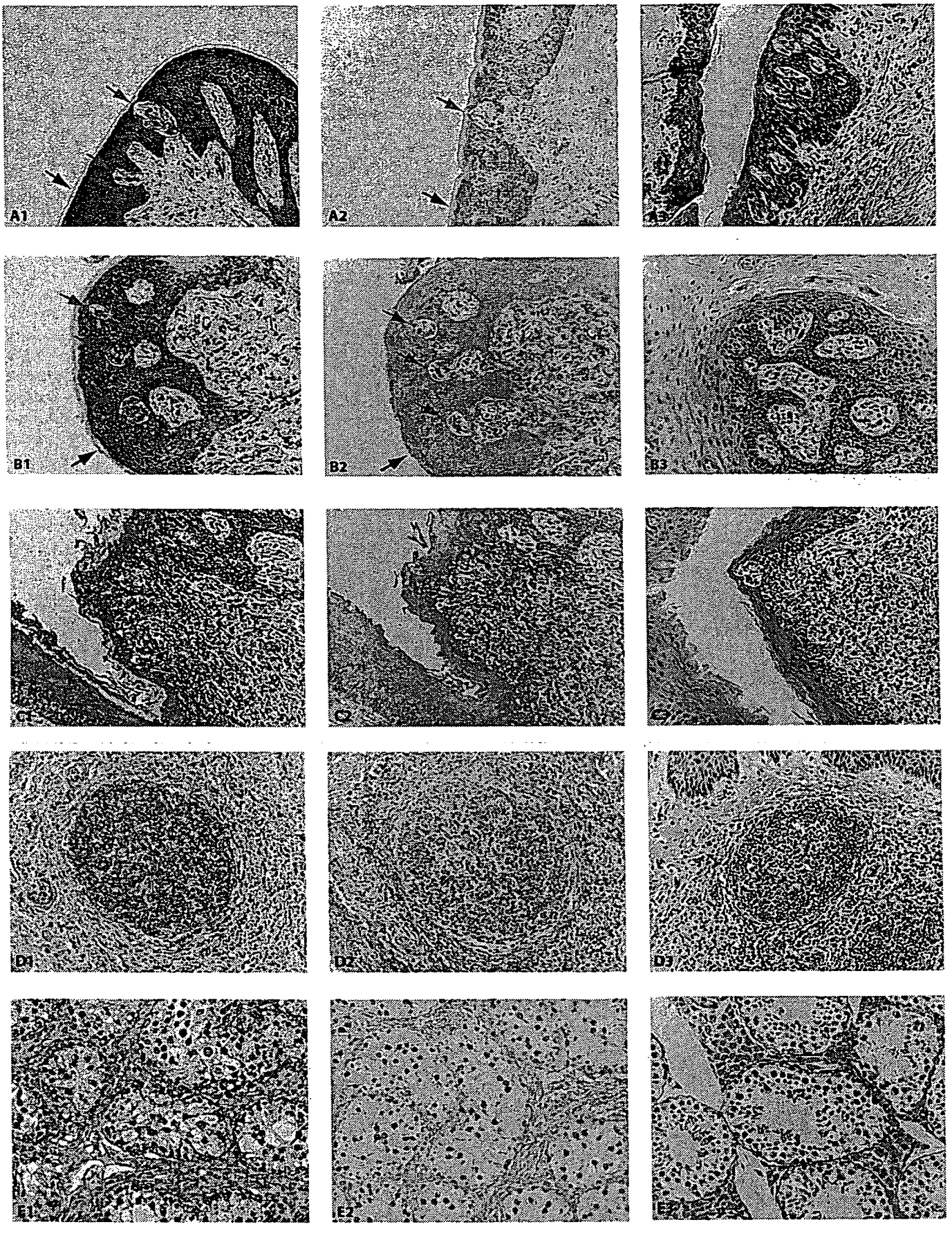
A1
A2
A3
B1
B2
B3
C1
C2
C3
D1
D2
D3
E1
E2
E3

to extract RNA from the lymphocytes. Real-time PCR using that RNA demonstrated the existence of a transcript from *TAS1R3* in B lymphocytes. However, since the amount of RNA prepared from the B lymphocytes was too small to be determined by UV absorbance, the amount of transcript in the B lymphocytes sample could not be directly compared with amounts of transcript in other samples (such as tongue). The DNA fragment amplified from B lymphocytes was cloned and sequenced, and found to be identical to that of *TAS1R3* cDNA. These findings confirmed the expression of *TAS1R3* in B lymphocytes, though the level of that expression could not be determined.

Exploitation of SNPs possibly related to tasting

The association between differences in sweet preference and sequence polymorphisms producing amino-acid substitutions has been previously reported in mouse (Max et al., 2001; Reed et al., 2004). Therefore, genomic DNAs from nine pigs of various breeds (see Materials and methods) were sequenced for the entire *TAS1R3* gene (position: 1055 to 6862 in the sequence with Accession No. AB162126), and the *TAS1R3* genomic sequences were compared. Eight SNPs in exons and five SNPs in introns were identified (described in the annotation of the sequence with Accession No. AB162126). However, no SNPs found in exons produced amino-acid substitutions (data not shown).

Discussion

TAS1R3 has been shown to be involved in sweet and umami tastes (along with TAS1R2 and TAS1R1) in mouse, and the sequence of the gene has been reported in mouse (Accession No. AL670236.9), rat (Accession No. NW_043877.1), gorilla (Accession No. AF545574), and human (Accession No. NT_077965.1). In the present study, the genomic structure of swine *TAS1R3* was determined, and *TAS1R3* expression was studied in various swine tissues. That gene was shown to reside on SSC6q22→q23, from which three distinct mRNA transcripts were generated: a 3,752-bp transcript derived from six exons was found in tongue, whereas in testis a 3,704-bp transcript from six exons, and a 3,630-bp transcript from seven exons were found. The 6-exons/5-introns structure was similar to those observed in human and mouse, but the 7-exons/6-introns structure of *TAS1R3* was first observed in swine. The expression pattern of the *TAS1R3* gene in tongue, testis, heart, lung, and liver was similar to that observed in mouse (Max et al., 2001). Additionally, a high expression with a level similar to that in testis was observed in kidney, a finding which had not previously been reported. In hybridization in situ, *TAS1R3* expression was detected in the tongue circumvallate papillae, fungiform papillae, mucosal epithelium, follicular B lymphocytes, lymphocytes in submucosal tissues of the lingual tonsil, and spermatogenic cells. In kidney, the expression appeared to be uniformly consistent rather than confined to specific cells. The expression of *TAS1R3* in B lymphocytes was further confirmed by real-time PCR using peripheral mature B lymphocytes, and by sequencing of the real-time PCR product.

Since the genomic structure, nucleotide sequence of cDNA, and amino-acid sequences of TAS1R3 are similar in swine, human and mouse, we hypothesized that functional transcription factor binding sites commonly exist in the three species. Based on this hypothesis, sequences upstream of the translation start site were compared to reveal an SRY binding site located 89 bp upstream of the translation start site as the one and only common site in the species. Hence, the SRY binding site is considered to serve as a functional binding site for the *TAS1R3* gene. However, in swine, two types of the exon/intron structures were involved in the generation of transcripts from *TAS1R3*, suggesting that another functional transcription factor binding site should exist. Genes such as the human collagen gene have previously been demonstrated to have functional transcription factor binding sites in their introns (Bornstein et al., 1987; Schultz et al., 1991). When the intron sequences of the three species were compared to identify common transcription factors, it was demonstrated that the Sp1 binding site was identified as a common site in swine and human intron 2. Therefore, it is possible that Sp1 would be another element in differential gene expression.

TAS1R3 expression was detected in the tongue circumvallate papillae, fungiform papillae, mucosal epithelium, follicular B lymphocytes, lymphocytes in submucosal tissues of the lingual tonsil, spermatogenic cells, kidney and peripheral mature B lymphocytes by both or either of real-time PCR and in situ hybridization. The expressions in circumvallate papillae and fungiform papillae were reported in mouse (Kitagawa et al., 2001; Max et al., 2001). However, expressions in tongue mucosal epithelium, kidney, and B lymphocytes have not been previously reported. In taste papillae, complexes of TAS1R1 and TAS1R3, and of TAS1R2 and TAS1R3 serve as the receptors for umami and sweet, respectively (Nelson et al., 2001, 2002). However, since no tasting function is considered to exist in tissues or cells other than the taste receptor cells, and since the types of cells expressing *TAS1R3* gene are different, it is possible that TAS1R3 is involved in different signal transductions in those cells via collaboration with proteins other than TAS1R1 and TAS1R2. In order to provide clues to infer the functions of *TAS1R3* in those cells, expressions of *TAS1R1* and *TAS1R2* should be examined specifically in those cells, while *TAS1R3* expression should be investigated throughout the differentiation processes of those cells.

Acknowledgements

The authors wish to thank Drs. Martine Yerle (INRA, France), Lawrence B. Schook (UIUC, USA), and Craig W. Beattie (UNR, USA) for supplying the IMpRH panel DNA. The authors also wish to thank Dr. Sue Galloway (AgResearch, New Zealand) for critical reading of our manuscript and suggestions in preparation of the manuscript.

References

Adler E, Hoon MA, Mueller KL, Chandrashekar J, Ryba NJ, Zuker CS: A novel family of mammalian taste receptors. Cell 100:693–702 (2000).

Awata T, Yamakuchi H, Kumagai M, Yasue H: Assignment of the tenascin gene *(HXB)* to swine chromosome 1q21.1→q21.3 by fluorescence in situ hybridization. Cytogenet Cell Genet 69: 33–34 (1995).

Bernhardt SJ, Naim M, Zehavi U, Lindemann B: Changes in IP3 and cytosolic Ca^{2+} in response to sugars and non-sugar sweeteners in transduction of sweet taste in the rat. J Physiol 490: 325–336 (1996).

Bornstein P, McKay J, Morishima JK, Devarayalu S, Gelinas RE: Regulatory elements in the first intron contribute to transcriptional control of the human alpha 1(I) collagen gene. Proc Natl Acad Sci USA 84:8869–8873 (1987).

Cummings TA, Daniels C, Kinnamon SC: Sweet taste transduction in hamster: sweeteners and cyclic nucleotides depolarize taste cells by reducing a K^+ current. J Neurophysiol 75:1256–1263 (1996).

Gilbertson TA, Avenet P, Kinnamon SC, Roper SD: Proton currents through amiloride-sensitive Na channels in hamster taste cells. Role in acid transduction. J Gen Physiol 100:803–824 (1992).

Gilbertson TA, Damak S, Margolskee RF: The molecular physiology of taste transduction. Curr Opin Neurobiol 10:519–527 (2000).

Kitagawa M, Kusakabe Y, Miura H, Ninomiya Y, Hino A: Molecular genetic identification of a candidate receptor gene for sweet taste. Biochem Biophys Res Commun 283:236–242 (2001).

Kiuchi S, Inage Y, Hiraiwa H, Uenishi H, Yasue H: Assignment of 280 swine genomic inserts including 31 microsatellites from BAC clones to the swine RH map (IMpRH map). Mamm Genome 13:80–88 (2002).

Kretz O, Barbry P, Bock R, Lindemann B: Differential expression of RNA and protein of the three pore-forming subunits of the amiloride-sensitive epithelial sodium channel in taste buds of the rat. J Histochem Cytochem 47:51–64 (1999).

Li X, Staszewski L, Xu H, Durick K, Zoller M, Adler E: Human receptors for sweet and umami taste. Proc Natl Acad Sci USA 99:4692–4696 (2002).

Lin W, Burks CA, Hansen DR, Kinnamon SC, Gilbertson TA: Taste receptor cells express pH-sensitive leak K^+ channels. J Neurophysiol 92: 2909–2919 (2004).

Lindemann B: Receptors and transduction in taste. Nature 413:219–225 (2001).

Max M, Shanker YG, Huang L, Rong M, Liu Z, Campagne F, Weinstein H, Damak S, Margolskee RF: *Tas1r3*, encoding a new candidate taste receptor, is allelic to the sweet responsiveness locus *Sac*. Nat Genet 28:58–63 (2001).

Mikawa S, Akita T, Hisamatsu N, Inage Y, Ito Y, Kobayashi E, Kusumoto H, Matsumoto T, et al: A linkage map of 243 DNA markers in an intercross of Gottingen miniature and Meishan pigs. Anim Genet 30:407–417 (1999).

Milan D, Hawken R, Cabau C, Leroux S, Genet C, Lahbib Y, Tosser G, Robic A, et al: IMpRH server: an RH mapping server available on the Web. Bioinformatics 16:558–559 (2000).

Nelson G, Hoon MA, Chandrashekar J, Zhang Y, Ryba NJ, Zuker CS: Mammalian sweet taste receptors. Cell 106:381–390 (2001).

Nelson G, Chandrashekar J, Hoon MA, Feng L, Zhao G, Ryba NJ, Zuker CS: An amino-acid taste receptor. Nature 416:199–202 (2002).

Ohtsuki T, Furuya S, Yamada T, Nomura S, Hata J, Yabe Y, Hosoda Y: Gene expression of noncollagenous bone matrix proteins in the limb joints and intervertebral disks of the *twy* mouse. Calcif Tissue Int 63:67–172 (1998).

Reed DR, Li S, Li X, Huang L, Tordoff MG, Starling-Roney R, Taniguchi K, West DB, et al: Polymorphisms in the taste receptor gene (*Tas1r3*) region are associated with saccharin preference in 30 mouse strains. J Neurosci 24:938–946 (2004).

Schultz JR, Tansey T, Gremke L, Storti RV: A muscle-specific intron enhancer required for rescue of indirect flight muscle and jump muscle function regulates *Drosophila* tropomyosin I gene expression. Mol Cell Biol 11:1901–1911 (1991).

Suzuki K, Asakawa S, Iida M, Shimanuki S, Fujishima N, Hiraiwa H, Murakami Y, Shimizu N, Yasue H: Construction and evaluation of a porcine bacterial artificial chromosome library. Anim Genet 31:8–12 (2000).

Suzuki Y, Sugano S: Construction of a full-length enriched and a 5'-end enriched cDNA library using the oligo-capping method. Methods Mol Biol 221:73–91 (2003).

Tumbelson ME, Schook LB: Advances in swine in biomedical research, in Tumbelson ME, Schook LB (eds): Advances in Swine in Biomedical Research, pp 1–4 (Plenum Press, New York 1996).

Yasue H, Ishibashi M: The oncogenicity of avian adenoviruses. III. In situ DNA hybridization of tumor line cells localized a large number of a virocellular sequence in few chromosomes. Virology 116:99–115 (1982).

Yerle M, Pinton P, Robic A, Alfonso A, Palvadeau Y, Delcros C, Hawken R, Alexander L, et al: Construction of a whole-genome radiation hybrid panel for high-resolution gene mapping in pigs. Cytogenet Cell Genet 82:182–188 (1998).

Zhao GQ, Zhang Y, Hoon MA, Chandrashekar J, Erlenbach I, Ryba NJ, Zuker CS: The receptors for mammalian sweet and umami taste. Cell 115:255–266 (2003).

Available online at www.sciencedirect.com
SCIENCE DIRECT
Leukemia Research 30 (2006) 1059–1062
Leukemia Research
www.elsevier.com/locate/leukres

Case report

Fulminant Epstein-Barr virus (EBV)-associated T-cell lymphoproliferative disorder with hemophagocytosis following autologous peripheral blood stem cell transplantation for relapsed angioimmunoblastic T-cell lymphoma

Norihiro Awaya[a,*], Akiko Adachi[a], Taisuke Mori[b], Hiroshi Kamata[a], Jin Nakahara[a], Kenji Yokoyama[a], Taketo Yamada[b], Masahiro Kizaki[a], Michiie Sakamoto[b], Yasuo Ikeda[a], Shin-ichiro Okamoto[a]

[a] *Division of Hematology, Department of Medicine, Keio University School of Medicine, Japan*
[b] *Department of Pathology, Keio University School of Medicine, Japan*

Received 23 September 2005; received in revised form 20 October 2005; accepted 23 October 2005
Available online 2 December 2005

Abstract

Post-transplant lymphoproliferative disorder (PTLD) is a complication that can develop after either solid-organ or hematopoietic stem cell transplantation (HSCT). T-cell PTLD is a rare disorder, especially following autologous HSCT. Here we report a case of T-cell PTLD which occurred after autologous peripheral blood stem cell transplantation (PBSCT) for relapsed angioimmunoblastic T-cell lymphoma (AILT). Three months after the transplant, the patient developed fever with elevated plasma Epstein-Barr virus (EBV)-PCR values. The patient subsequently developed pneumonitis, hepatomegaly and marked pancytopenia due to hemophagocytosis. The patient died of multi-organ failure, despite antiviral and steroid pulse therapy. Our post-mortem study confirmed the marked proliferation of EBV-infected T-cells that differed from the original AILT clone and macrophages/histiocytes were observed in the marrow, liver, lymph nodes and lungs. Phagocytosis was most evident in the bone marrow. The patient's AILT remained in complete remission. To the best of our knowledge, this is the first case of fulminant EBV-associated T-cell lymphoproliferative disorder (LPD) following autologous HSCT.

Keywords: Epstein-Barr virus; T-cell lymphoproliferative disorder; Hemophagocytosis; Autologous peripheral blood stem cell transplantation; Angioimmunoblastic T-cell lymphoma

1. Introduction

PTLD occurs as a consequence of immunosuppression in a solid-organ or hematopoietic allograft recipient. The overall incidence of PTLD following solid-organ transplant and standard T-cell repleted allogeneic bone marrow transplant is 1–3% [1] and has rarely been reported after autologous HSCT [2]. PTLD consists of a spectrum of disorders ranging from EBV-driven polyclonal proliferation resembling infectious mononucleosis to clonal EBV-positive B-cell lymphoma. In contrast to B-cell PTLD, T-cell PTLD is less frequent and is not usually associated with EBV [3]. Here, we report the case which developed clonal EBV-associated T-cell proliferation with hemophagocytosis following autologous PBSCT for relapsed AILT. This clinical presentation was compatible with previously reported fulminant T-cell LPD [4].

2. Case report

A 49-year-old Japanese male initially noticed lymphadenopathy in the right groin in December 2001, which

* Corresponding author at: 35 Shinanomachi, Shinjuku-ku, Tokyo 160-8582, Japan. Tel.: +81 3 5363 3785; fax: +81 3 3353 3515.
E-mail address: nawaya@sc.itc.keio.ac.jp (N. Awaya).

0145-2126/$ – see front matter © 2005 Elsevier Ltd. All rights reserved.
doi:10.1016/j.leukres.2005.10.022

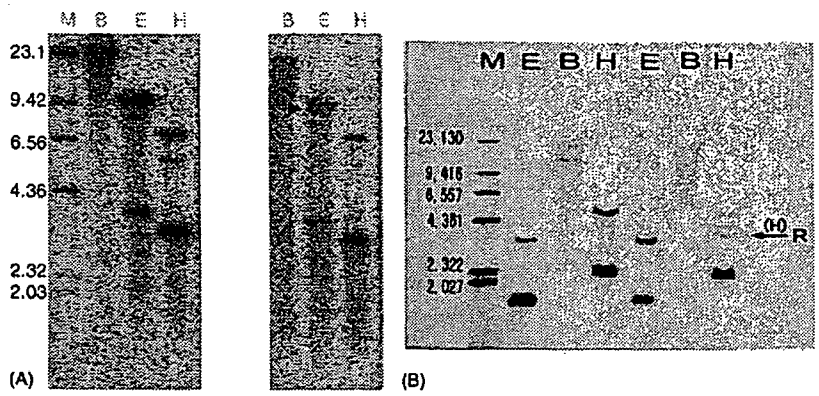

Fig. 1. Southern blot analysis for TCR gene rearrangement. (A) TCR β was positive when T-cell LPD developed after autologous HSCT. (B) In contrast, TCR γ was detected at the time of the initial diagnosis. The three left lanes serve as controls and the three right lanes represent patient samples in both experiments. M: molecular size marker (λDNA/Hind III), E: EcoR I, B: BamH I, H: Hind III.

spontaneously regressed without treatment. He later presented with recurring bilateral inguinal lymphadenopathy in November 2002 and the histological findings of a biopsy specimen from the right inguinal node were compatible with AILT. In situ hybridization for EBV-encoded small nuclear RNAs (EBER) and latent membrane protein (LMP) was positive and notably, EBER was detected in both the B- and T-cell populations. Complete remission was achieved after five cycles of CHOP (cyclophosphamide, doxorubicin, vincristine and prednisolone). Relapse was histologically confirmed when left cervical lymph node swelling developed in February 2004. Salvage chemotherapy (ESHAP; etoposide, cytarabine, cisplatin and methylprednisolone) was administered and 8.4×10^6/kg of G-CSF mobilized peripheral CD34-positive cells were collected from the patient and were cryopreserved. The patient was subsequently treated with MCVAC (ranimustine, cytarabine, etoposide and cyclophosphamide) and received autologous PBSCT in June 2004. The treatment course was only complicated with a low-grade fever for 2 weeks starting on day 27 post-transplant. The fever was

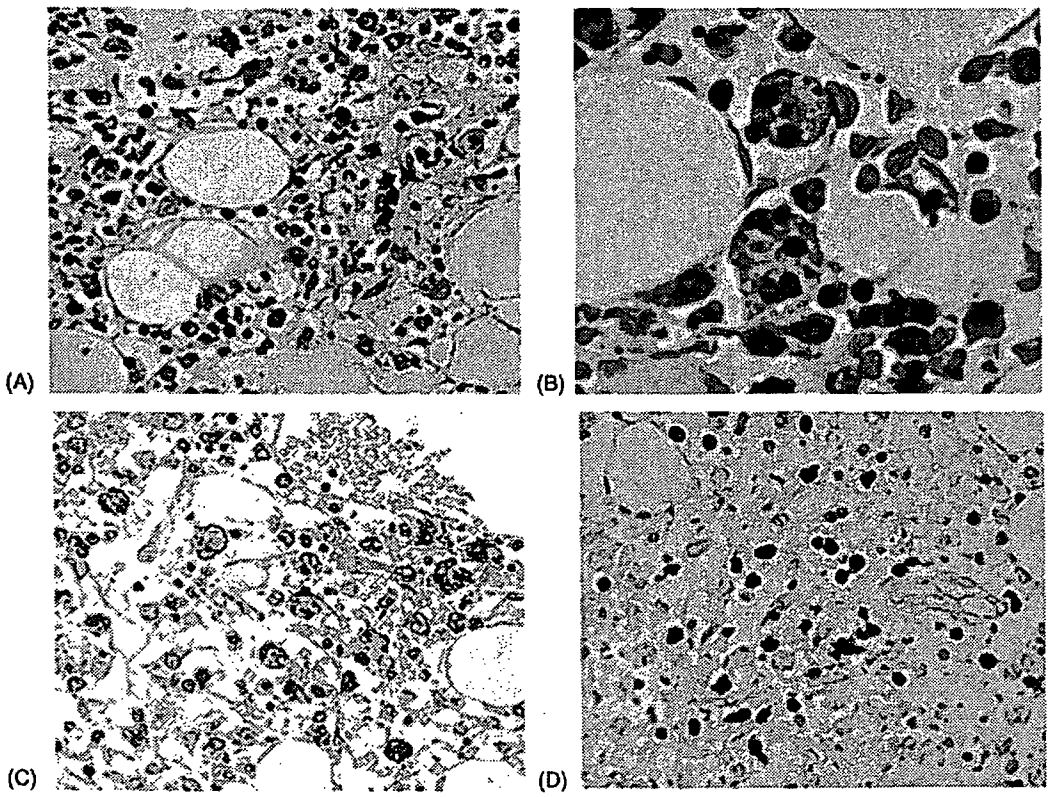

Fig. 2. Histological findings of the bone marrow at autopsy. (A) Hemophagocytosis was evident (hematoxylin and eosin, ×200). (B) High-power field (×1000). (C) Phagocytic cells were CD68-positive (×200). (D) EBER hybridization for CD3-positive cells (×200).

associated with a high EBV-PCR value of 10,000 copies/ml. The patient subsequently became afebrile and the EBV-PCR value decreased to 200 copies/ml without any antiviral treatment. In September 2004, he presented with fever and superficial lymphadenopathy. Laboratory data showed elevated values of lactate dehydrogenase (LDH), soluble interleukin-2 receptor (sIL-2R) and EBV-PCR (1000 copies/ml). Transient amelioration of fever and lymphadenopathy occurred after the administration of valaciclovir. Nevertheless, interstitial pneumonitis developed in October, in addition to the abovementioned abnormalities and the patient was admitted to our hospital in November. On admission, physical examination revealed a temperature of 38.3 °C, fine crackles to auscultation of the lungs, superficial lymphadenopathy of up to 1 cm in diameter and hepatomegaly palpated 2 cm below the right costal margin. Laboratory values on admission were as follows: white blood cells 2600/μl, hemoglobin 10.5 g/dl, platelet count 4.9×10^4/μl, LDH 522 IU/l, sIL-2R 4330 U/ml, IgG 918 mg/dl and EBV-PCR 9000 copies/ml. The patient was again placed on valaciclovir; however, the fever and lymphadenopathy persisted, with the subsequent development of pancytopenia, which required both packed red cell as well as platelet transfusion. Serum ferritin and triglyceride levels were also elevated. Treatment with foscarnet and high-dose steroids was ineffective and the patient died of multi-organ failure. The LDH, sIL-2R and EBV-PCR values just prior to the patient's death were 10,140 IU/l, 32,300 U/ml and 20,000 copies/ml, respectively. Permission for autopsy was granted. Autopsy revealed the presence of CD3-positive cells in the marrow, portal area of the liver, lymph nodes and lungs and those cells were also positive for EBER, as determined by serial sections. DNA rearrangement of T-cell receptor (TCR) β was positive (Fig. 1A); however, no DNA rearrangement for TCR γ was detected, although tests for this rearrangement had originally been positive at the time of the initial diagnosis of AILT (Fig. 1B). CD3-positive cells did not express CD4 (data not shown), which was positive for the original AILT cells. These findings suggested that these EBV-infected T-cells were derived from T-cell clones that differed from the original AILT clone and that the patient's AILT had remained in remission. Another significant finding of this case was the presence of hypocellularity in the marrow, which was associated with the proliferation of CD68-positive macrophages and marked hemophagocytosis (Fig. 2A–C). CD68-positive macrophages were also noticeable in the liver, lymph nodes and lungs. Again, EBER was positive for T-cells in the marrow (Fig. 2D).

3. Discussion

PTLD represents a spectrum of EBV-related clinical diseases, from a polyclonal mononucleosis-like illness to a monomorphic disease with sufficient cytologic and architectural atypia to be diagnosed as a lymphoma. In patients who undergo solid-organ transplantation, high-levels of immunosuppression are considered as a risk factor and the incidence of PTLD has been reported to approach 10% in lung transplant patients, where high-levels of immunosuppression are required [5]. Generally, the risk of PTLD is between 1 and 3% in recipients of organ transplant or T-cell repleted allogeneic HSCT [1,5]. In contrast, only a few cases have been described of EBV-associated PTLD following autologous HSCT [6–8]. Yufu et al. reported the first case of EBV-associated T-cell PTLD following autologous PBSCT for relapsed Hodgkin's disease [2]. In contrast to the present case, the patient described in their report presented with clonal CD8-positive cell proliferation and had a clinical course similar to that of chronic active EBV infection. The clinical features of our case were more similar to those of patients with fulminant T-cell LPD described by Quintanilla-Martinez et al. [4]. The latter cases were characterized by fever, liver failure, pancytopenia secondary to hemophagocytosis, hepatosplenomegaly and many showed no significant lymphadenopathy. The clinical course was literally fulminant and most of the patients died within days to months [4]. Also in their cases, EBV infected T-cell clones were detected in the liver, spleen, or lymph nodes. Our post-mortem study also clearly demonstrated a correlation with EBV positivity, as determined by EBER hybridization, with CD3 staining.

EBV is capable of infecting not only B-cells, but also T-cells and natural killer (NK) cells and it is known to cause LPD or lymphoma [4,9,10]; however, most PTLDs are of B-cell origin and are associated with EBV infection. Approximately 4–14% of adult PTLDs are of T-cell origin, which is rarely associated with EBV infection and to date, only 14 cases have been reported [1,11,12]. Interestingly, a phenotype switch between the B- and T-cell types has been described in a single case with immunodeficiency [13]. Our case showed the coexistence of infected B- and T-cell populations at the initial presentation of the disease, which appears to be a characteristic of AILT [14]. AILT itself is known to be susceptible for the development of B-LPD [15]; however, the factors responsible for influencing the lineage commitment of LPD remain undetermined at present. In the present patient, no recurrence of AILT was observed, as based on the lack of CD4 expression, as well as on the absence of TCR γ rearrangement, both of which had originally been present at the time of the patient's initial diagnosis of AILT. As regards T-cell PTLD with hemophagocytosis, only a single post-liver transplantation pediatric case has been reported to date [16]. To the best of our knowledge, this is the first case reported in the literature of fulminant T-cell PTLD with hemophagocytosis following autologous HSCT.

One of the treatment options for PTLD following solid-organ transplantation or allogeneic HSCT would be the withdrawal of immunosuppressive therapy. However, such an approach would not be applicable for PTLD after autologous HSCT. Antiviral thymidine kinase inhibitors, ganciclovir and acyclovir, are theoretically ineffective against EBV in vivo, because EBV survives as an episome outside of the lymphocytic genome. It was of note that a transient effect of

valaciclovir was observed in the present case; moreover, a similar clinical course was previously obtained with valaciclovir treatment [17]. Further investigation in a combination of EBV-PCR monitoring and the preemptive use of valaciclovir might be warranted in cases of AILT after autologous HSCT.

Acknowledgments

The authors would like to thank the nurses in the ward, Dr. Mariko Yabe, Dr. Yuiko Tsukada, Dr. Takayuki Shimizu, Dr. Toyotaka Iguchi, Dr. Chien-Kang Chen, Dr. Akihiro Yokoyama and Dr. Takehiko Mori for their excellent care to the patient.

Contributions. N. Awaya provided drafting of the manuscript and important intellectual content. A. Adachi, H. Kamata and J. Nakahara collected and organized the data. T. Mori, T. Yamada and M. Sakamoto examined and provided pathological materials. T. Mori was responsible for autopsy reports. K. Yokoyama, M. Kizaki and Y. Ikeda provided critical revisions. S. Okamoto provided critical revisions and gave final approval.

References

[1] Lundell R, Elenitoba-Johnson KS, Lim MS. T-cell post-transplant lymphoproliferative disorder occurring in a pediatric solid-organ transplant patient. Am J Surg Pathol 2004;28:967–73.

[2] Yufu Y, Kimura M, Kawano R, Noguchi Y, Takatsuki H, Uike N, et al. Epstein-Barr virus-associated T-cell lymphoproliferative disorder following autologous blood stem cell transplantation for relapsed Hodgkin's disease. Bone Marrow Transpl 2000;26:1339–41.

[3] Bhatia S, Ramsay NK, Steinbuch M, Dusenbery KE, Shapiro RS, Weisdorf DJ, et al. Malignant neoplasms following bone marrow transplantation. Blood 1996;87:3633–9.

[4] Quintanilla-Martinez L, Kumar S, Fend F, Reyes E, Teruya-Feldstein J, Kingma DW, et al. Fulminant EBV(+) T-cell lymphoproliferative disorder following acute/chronic EBV infection: a distinct clinicopathologic syndrome. Blood 2000;96:443–51.

[5] Loren AW, Porter DL, Stadtmauer EA, Tsai DE. Post-transplant lymphoproliferative disorder: a review. Bone Marrow Transpl 2003;31: 145–55.

[6] Shepherd JD, Gascoyne RD, Barnett MJ, Coghlan JD, Phillips GL. Polyclonal Epstein-Barr virus-associated lymphoproliferative disorder following autografting for chronic myeloid leukemia. Bone Marrow Transpl 1995;15:639–41.

[7] Hauke RJ, Greiner TC, Smir BN, Vose JM, Tarantolo SR, Bashir RM, et al. Epstein-Barr virus-associated lymphoproliferative disorder after autologous bone marrow transplantation: report of two cases. Bone Marrow Transpl 1998;21:1271–4.

[8] Lones MA, Kirov I, Said JW, Shintaku IP, Neudorf S. Post-transplant lymphoproliferative disorder after autologous peripheral stem cell transplantation in a pediatric patient. Bone Marrow Transpl 2000;26:1021–4.

[9] Kawa K. Epstein-Barr virus-associated diseases in humans. Int J Hematol 2000;71:108–17.

[10] Kasahara Y, Yachie A, Takei K, Kanegane C, Okada K, Ohta K, et al. Differential cellular targets of Epstein-Barr virus (EBV) infection between acute EBV-associated hemophagocytic lymphohistiocytosis and chronic active EBV infection. Blood 2001;98:1882–8.

[11] Leblond V, Davi F, Charlotte F, Dorent R, Bitker MO, Sutton L, et al. Post-transplant lymphoproliferative disorders not associated with Epstein-Barr virus: a distinct entity? J Clin Oncol 1998;16: 2052–9.

[12] Nelson BP, Nalesnik MA, Bahler DW, Locker J, Fung JJ, Swerdlow SH. Epstein-Barr virus-negative post-transplant lymphoproliferative disorders: a distinct entity? Am J Surg Pathol 2000;24:375–85.

[13] Imashuku S, Miyagawa A, Chiyonobu T, Ishida H, Yoshihara T, Teramura T, et al. Epstein-Barr virus-associated T-lymphoproliferative disease with hemophagocytic syndrome, followed by fatal intestinal B-lymphoma in a young adult female with WHIM syndrome. Warts, hypogammaglobulinemia, infections and myelokathexis. Ann Hematol 2002;81:470–3.

[14] Anagnostopoulos I, Hummel M, Finn T, Tiemann M, Korbjuhn P, Dimmler C, et al. Heterogeneous Epstein-Barr virus infection patterns in peripheral T-cell lymphoma of angioimmunoblastic lymphadenopathy type. Blood 1992;80:1804–12.

[15] Zettl A, Lee SS, Rudiger T, Starostik P, Marino M, Kirchner T, et al. Epstein-Barr virus-associated B-cell lymphoproliferative disorders in angioimmunoblastic T-cell lymphoma and peripheral T-cell lymphoma, unspecified. Am J Clin Pathol 2002;117:368–79.

[16] George TI, Jeng M, Berquist W, Cherry AM, Link MP, Arber DA. Epstein-Barr virus-associated peripheral T-cell lymphoma and hemophagocytic syndrome arising after liver transplantation: case report and review of the literature. Pediatr Blood Cancer 2005;44:270–6.

[17] Battegay M, Berger C, Rochlitz C, Hurwitz N, Hirsch HH, De Geyter C, et al. Epstein-Barr virus load correlating with clinical manifestation and treatment response in a patient with angioimmunoblastic T-cell lymphoma. Antivir Ther 2004;9:453–9.

1′-Acetoxychavicol Acetate Is a Novel Nuclear Factor κB Inhibitor with Significant Activity against Multiple Myeloma *In vitro* and *In vivo*

Keisuke Ito,[1] Tomonori Nakazato,[1] Ming Ji Xian,[1] Taketo Yamada,[2] Nobumichi Hozumi,[3] Akira Murakami,[4] Hajime Ohigashi,[4] Yasuo Ikeda,[1] and Masahiro Kizaki[1]

[1]Division of Hematology, Department of Internal Medicine and [2]Pathology, Keio University School of Medicine, Tokyo, Japan; [3]Institute of Biological Science, Science University of Tokyo, Chiba, Japan; and [4]Division of Food Science and Biotechnology, Graduate School of Agriculture, Kyoto University, Kyoto, Japan

Abstract

1′-Acetoxychavicol acetate (ACA) is a component of a traditional Asian condiment obtained from the rhizomes of the commonly used ethno-medicinal plant *Languas galanga*. Here, we show for the first time that ACA dramatically inhibits the cellular growth of human myeloma cells via the inhibition of nuclear factor κB (NF-κB) activity. In myeloma cells, cultivation with ACA induced G_0-G_1 phase cell cycle arrest, followed by apoptosis. Treatment with ACA induced caspase 3, 9, and 8 activities, suggesting that ACA-induced apoptosis in myeloma cells mediates both mitochondrial- and Fas-dependent pathways. Furthermore, we showed that ACA significantly inhibits the serine phosphorylation and degradation of IκBα. ACA rapidly decreased the nuclear expression of NF-κB, but increased the accumulation of cytosol NF-κB in RPMI8226 cells, indicating that ACA inhibits the translocation of NF-κB from the cytosol to the nucleus. To evaluate the effects of ACA *in vivo*, RPMI8226-transplanted NOD/SCID mice were treated with ACA. Tumor weight significantly decreased in the ACA-treated mice compared with the control mice. In conclusion, ACA has an inhibitory effect on NF-κB, and induces the apoptosis of myeloma cells *in vitro* and *in vivo*. ACA, therefore, provides a new biologically based therapy for the treatment of multiple myeloma patients as a novel NF-κB inhibitor. (Cancer Res 2005; 65(10): 4417-24)

Introduction

1′-Acetoxychavicol acetate (ACA) is obtained from the rhizomes of *Languas galanga* (Zingiberaceae), a traditional condiment in Thailand (1). Recent studies have revealed that ACA has potent chemopreventive effects against rat oral carcinomas and inhibits the chemically induced tumor formation and cellular growth of various cancer cells (2–5). More recently, we reported that ACA induces the apoptosis of myeloid leukemia cells *in vitro* and *in vivo*, suggesting that ACA has potential as a novel therapeutic agent for the treatment of myeloid leukemia (6). We found that the ACA-induced apoptosis in myeloid leukemic cells was associated with the production of intracellular reactive oxygen species (ROS; ref. 6); however, the exact biological and molecular mechanisms of ACA-induced apoptosis in various cancer cells are still unclear.

Multiple myeloma is a plasma cell malignancy that remains incurable despite the use of conventional and high-dose chemotherapy with hematopoietic stem cell transplantation; therefore, novel therapeutic approaches are urgently needed in clinical settings (7). The understanding that has recently been gained into the biology of myeloma has led to the development of biological treatments, such as thalidomide and bortezomib, which target the myeloma cell and the bone marrow microenvironment. These agents have shown remarkable activity against refractory multiple myeloma in early clinical trials, but prolonged drug exposure may result in the development of *de novo* drug resistance in some cases (7–9). Therefore, the identification and validation of additional novel targeted therapies to overcome drug resistance and improve patient outcome are needed.

Nuclear factor κB (NF-κB), which was originally identified as a B-cell nuclear factor, is required for the proper regulation of B-cell homeostasis (10, 11). NF-κB is a member of the Rel family of proteins, and is typically a heterodimer composed of p50, p65, and IκBα subunits. NF-κB is constitutively present in the cytosol and is inactivated by its interaction with IκB family inhibitors. On activation, IκBα undergoes phosphorylation and ubiquitination-dependent degradation by the 26S proteosome, leading to translocation of NF-κB into the nucleus and binding to the specific DNA sequences in the promoter of the target genes, which stimulates their transcription (12–14). The protein products of these genes, including a variety of cytokines, cell adhesion molecules, and chemokines, mediate the regulation of cellular growth in many cells. Recently, it has been reported that NF-κB is constitutively active in myeloma cells, which contributes to the survival of these cells (15, 16). In addition, it has been reported that myeloma cell adhesion to bone marrow stromal cells induces NF-κB–dependent up-regulation of the transcription of IL-6, a major growth factor of myeloma cells (17). Tumor necrosis factor (TNF)-α is secreted into the bone marrow microenvironment and induces NF-κB–dependent alteration in adhesion molecule expression in both myeloma cells and bone marrow stromal cells, with resulting increased cell adhesion. This confers resistance to myeloma cell apoptosis and also triggers the NF-κB–dependent secretion of IL-6. These results indicate that NF-κB is the most important therapeutic target for the treatment of multiple myeloma. Conventional and recent antimyeloma agents, including dexamethasone, thalidomide, proteasome inhibitor PS-341, and arsenic trioxide, inhibit

Requests for reprints: Masahiro Kizaki, Division of Hematology, Department of Internal Medicine, Keio University School of Medicine, 35 Shinanomachi, Shinjuku-ku, Tokyo 160-8582, Japan. Phone: 81-3-5363-3785; Fax: 81-3-3353-3515; E-mail: makizaki@sc.itc.keio.ac.jp.

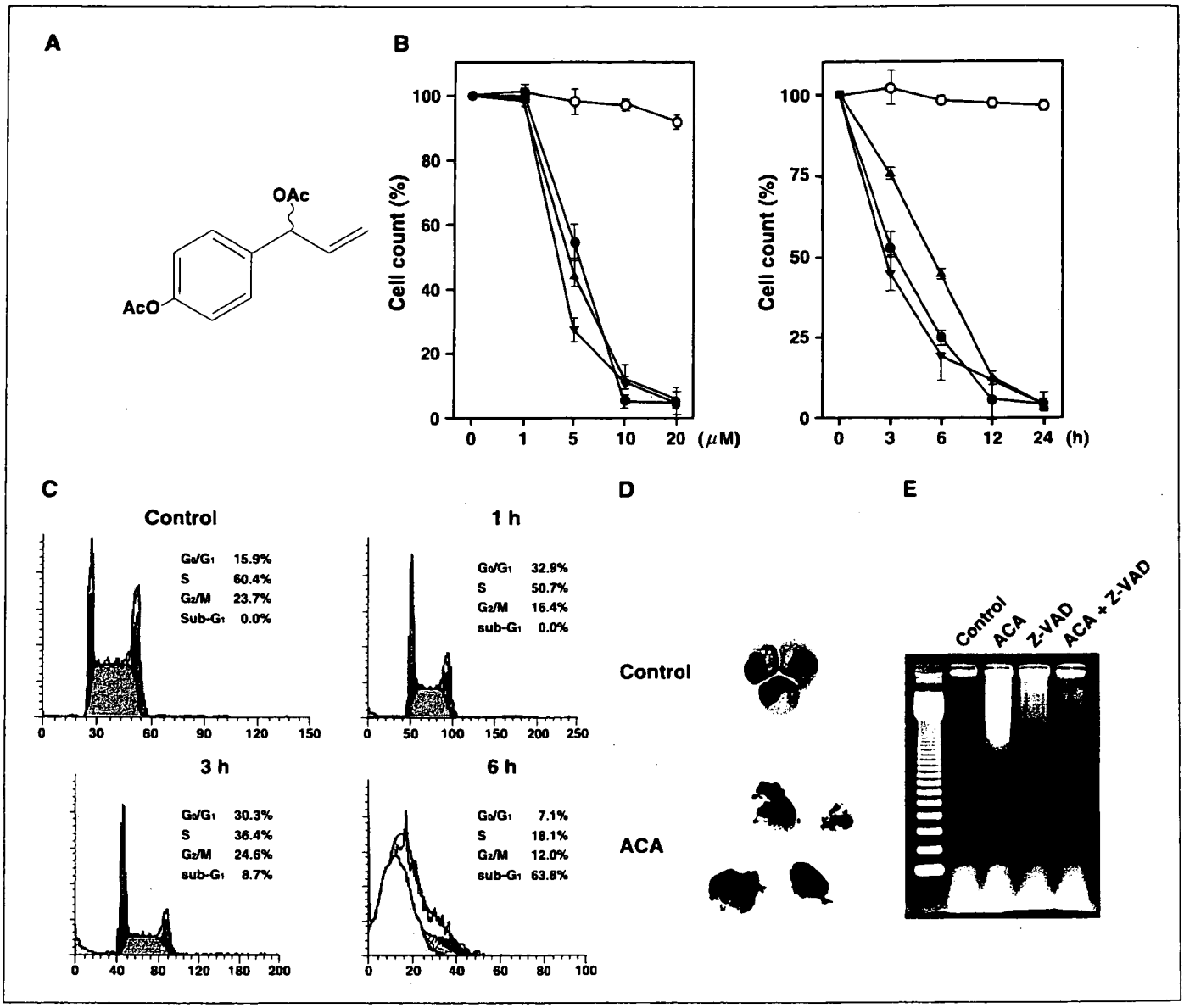

Figure 1. Chemical structure of ACA and induction of G_0-G_1 cell cycle arrest followed by apoptosis in various myeloma cells. *A*, chemical structure of (1′*R*, *S*′)-ACA. *B* and *C*, various myeloma cell lines [RPMI8226 (●), U266 (▲), IM-9 (▼) and bone marrow mononuclear cells from a healthy donor (○)] were treated with various concentrations (0-20 μmol/L) of ACA for 24 hours (*B*, *left*) and with 10 μmol/L ACA for various times (0-24 hours; *B*, *right*). Cell viability was assessed by trypan blue dye exclusion. Results are expressed as the mean ± SD of three different experiments. *C*, cell cycle analysis. RPMI8226 cells were treated with 10 μmol/L ACA for the indicated times, and then stained with PI as described in Materials and Methods. The DNA content was analyzed by means of flow cytometry. G_0-G_1, S, and G_2-M indicate the cell phase, and the sub-G_1 DNA content refers to the portion of apoptotic cells. Each phase was calculated by using a ModiFIT program. Three duplicate experiments were done with similar results, and the representative data are shown. *D*, morphologic changes characteristic of apoptosis in RPMI8226 cells. RPMI8226 cells were treated with 10 μmol/L ACA for 3 hours, and cytospin slides were then prepared and stained with Giemsa. Original magnification, ×1,000. *E*, agarose gel electrophoresis demonstrating DNA fragmentation in RPMI8226 cells treated with 10 μmol/L ACA for 3 hours. Preincubation with 20 μmol/L pan-caspase inhibitor, Z-VAD-FMK, inhibited ACA-induced apoptosis.

NF-κB activation (18–21). However, these agents have a multiple number of other biological effects. Therefore, a more specific NF-κB inhibitor may have clinical benefits and the blockade of its signaling pathway may represent a novel therapeutic strategy for managing multiple myeloma.

Our previous study showed that ACA induces apoptosis through two different pathways in the myeloid leukemia cells: ROS generation and the activation of the Fas-pathway (6). NF-κB is known to contribute to both the caspase 8 and 9 pathways. In this study, we addressed the molecular mechanisms of the antimyeloma action of ACA, and, quite surprisingly, we found that ACA inhibited the cellular growth of myeloma cells in association with the down-regulation of NF-κB activity. We further investigated the molecular mechanism of ACA and the possibility of clinically applying it by using *in vivo* mice model.

Materials and Methods

Cell cultures. Various human multiple myeloma cell lines, including RPMI8226, U266, and IM-9, were obtained from the Japan Cancer Research Resources Bank (Tokyo, Japan), and were maintained in RPMI 1640 (GIBCO-BRL, Grand Island, NY) with 10% fetal bovine serum (GIBCO-BRL),

100 units/mL penicillin, and 100 mg/mL streptomycin in a humidified atmosphere with 5% CO_2. Bone marrow samples from patients with multiple myeloma and healthy donors were obtained according to appropriate Human Protection Committee validation at Keio University School of Medicine (Tokyo, Japan), and with written informed consent. The patients' samples were grown in RPMI 1640 with 15% FBS (Hyclone Laboratories, Logan, MT) under standard culture conditions.

Reagents. ACA (99% purity) was synthesized as previously reported (Fig. 1*A*; ref. 1). Synthetic (1′*R*, *S*′)-ACA has an identical suppressive activity to natural (1′*S*)-ACA, as evaluated by tumor promoter–induced EBV activity (22). ACA was dissolved in DMSO at a stock concentration of 20 mmol/L. Various caspase inhibitors, including Z-VAD-FMK (a pan-caspase inhibitor), DEVD-FMK (a caspase 3 inhibitor), Z-IETD-FMK (a caspase 8 inhibitor), and LEHD-FMK (a caspase 9 inhibitor), were purchased from Calbiochem (La Jolla, CA). TNF-α was purchased from Sigma Chemical (St. Louis, MO). Phorbol 12-myristate 13-acetate (PMA: synthetic analogue of diacylglycerol) was dissolved in DMSO. The final DMSO concentrations in the medium were not greater than 0.1%. *N*-Tosyl-L-lysine chloromethyl ketone (TLCK), a serine protease inhibitor, was obtained from Roche (Indianapolis, IN). MG132 (z-Leu-Leu-Leu-aldehyde), a proteasome inhibitor, was purchased from BIOMOL Research Laboratories, Inc. (Plymouth Meeting, PA). For the Fas inhibition assay, antagonistic anti-ZB4 monoclonal antibody was purchased from MBL (Nagoya, Aichi, Japan).

Assays for apoptosis. Apoptosis was determined based on morphologic changes. Apoptotic cells were quantified by annexin V-FITC and propidium iodide (PI) double staining using a staining kit purchased from PharMingen (San Diego, CA). The induction of apoptosis was also detected by DNA fragmentation assay.

Western blot analysis. The cells were collected by centrifugation at 700 × *g* for 10 minutes, and then the pellets were resuspended in a lysis buffer [1% NP40, 1 mmol/L phenylmethylsulfonyl fluoride, 40 mmol/L Tris-HCl (pH 8.0), 150 mmol/L NaCl] at 4°C for 15 minutes. Mitochondrial and cytosolic fractions were prepared with digitonin-nagarse treatment. Protein concentrations were determined using a protein assay DC system (Bio-Rad, Richmond, CA). Cell lysates (15 μg of protein per lane) were fractionated on 12.5% SDS-polyacrylamide gels before being transferred to the membrane (Immobilon-P membranes, Millipore, Bedford, MA) according to standard protocol. Antibody binding was detected by using the enhanced chemiluminescence kit with hyper-ECL film (Amersham, Buckinghamshire, United Kingdom). The blots were also stained with Coomassie brilliant blue to confirm that equal amounts of protein extract were presented in each lane. The following antibodies were used in this study: anti-Fas (PharMingen); IκBα, pSer32-IκBα (Cell Signaling Technology, Inc., Beverly, MA); intercellular adhesion molecule 1 (ICAM-1), NF-κB, FLICE-inhibitory protein (FLIP), X-linked inhibitor of apoptosis protein (XIAP), apoptosis inducing factor (AIF), caspase inhibitory protein-1 (cIAP), and β-actin (Santa Cruz Biotech, Santa Cruz, CA).

Assays for nuclear factor κB activity. The DNA binding activity of NF-κB in the myeloma cells was quantified by ELISA using the Trans-NF-κB p65 Transcription Factor Assay Kit (Active Motif North America, Carlsbad, CA), according to the instructions of the manufacturer. Briefly, nuclear extracts were prepared and incubated in 96-well plates coated with immobilized oligonucleotide (5′-AGTTGAGGGGACTTTCCCAGGC-3′) containing a consensus (5′-GGGACTTTC-3′) binding site for the p65 subunit of NF-κB. NF-κB binding to the target oligonucleotide was detected by incubation with the primary antibody specific for the activation form of p65 (Active Motif North America), visualized by anti-immunoglobulin G horseradish peroxidase conjugate and Developing Solution, and quantified at 450 nm with a reference wavelength of 655 nm. Background binding, obtained by incubation with a 2-nucleotide mutant oligonucleotide (5′-AGTTGAGGCCACTTTCCCAGGC-3′), was subtracted from the value obtained for binding to the consensus DNA sequence.

Effects of 1′-acetoxychavicol acetate *in vivo*. We have established a human leukemia and multiple myeloma model in an NOD/SCID mouse (23). Briefly, the mice were pretreated with 3 Gy of total body irradiation, which is a sublethal dose that was expected to enhance the acceptance of xenografts. Subsequently, RPMI8226 cells (1×10^7 cells) in their logarithmic growth phase were inoculated s.c. into the NOD/SCID mice (Jackson Laboratory, Bar Harbor, ME). The inoculated RPMI8226 cells formed s.c. tumors at the injection site, and the cells grew rapidly. Seven days after the implantation of the cells, the mice with the transplanted cells were randomly assigned to receive PBS ($n = 10$) or 3 mg/kg ACA ($n = 10$) as an i.p. injection once every 3 days for 2 weeks. After 2 weeks of treatment, the mice were sacrificed and dissected to measure the tumor weights. When the mice showed severe wasting, or when the observations were completed, the mice were sacrificed according to the UKCCCR guidelines, and the day of sacrifice was recorded (24).

Results

Effects of 1′-acetoxychavicol acetate on cellular proliferation of various myeloma cells. We first investigated the effects of ACA on the cellular proliferation of three human multiple myeloma cell lines, including RPMI8226, U266, and IM-9 cells, and fresh samples from patients with multiple myeloma. ACA induced

Table 1. Clinical characteristics and the effects of ACA on the induction of apoptosis and NF-κB activity in eight patients with multiple myeloma

Patient	Age (y)/Sex	Bone marrow plasma cells (%)	Annexin V–positive cells (%)			NF-κB activity (%)
			Control	ACA	Fold increase	
1	73/M	78.6	5.6	93.5	16.7	43.3
2	54/M	75.6	6.8	84.3	12.4	50.5
3	70/M	55.2	4.6	87.6	19.0	46.2
4	58/F	46.4	10.4	75.4	7.3	41.5
5	61/F	78.5	7.4	80.4	10.9	57.4
6	34/F	63.5	8.3	81.1	9.8	60.1
7	46/M	57.6	12.2	92.5	7.6	42.1
8	75/M	48.2	9.3	78.5	8.4	38.5

NOTE: Fresh myeloma cells from patients were separated by Lymphoprep sedimentation procedure and subsequently cultured with 10 μmol/L of ACA. Induction of apoptosis was examined by annexin V–positive cells. The DNA binding activity of NF-κB was quantified by ELISA with the use of the Trans-AM NF-κB p65 Transcriptional Factor Assay Kit, and results were expressed as the percentage of the control cells.

apoptosis of myeloma cell lines, as well as of eight freshly obtained samples from patients with multiple myeloma, but not of normal bone marrow mononuclear cells from a healthy donor, in a dose- and time-dependent manner (Fig. 1*B*; Table 1). Cultivation with ACA rapidly and strongly increased the population of RPMI8226 myeloma cells in the G_0-G_1 phase, and then in the sub-G_1 phase (Fig. 1*C*). Apoptosis was assessed in terms of both the morphologic changes and the DNA ladder formation (Fig. 1*D* and *E*). Consistent with these results, annexin V–positive cells were increased after incubation with ACA for 3 hours, indicating that the onset of apoptosis had already started to occur after only 3 hours of treatment (data not shown). These results indicate that ACA led to cell cycle arrest at the G_0-G_1 phase, followed by apoptosis.

Effects of 1′-acetoxychavicol acetate on caspase activity. Treatment with 10 μmol/L ACA for 3 hours significantly induced caspase 3, 8, and 9 activities in RPMI8226 cells (Fig. 2*A*). RPMI8226 cells were treated with 10 μmol/L ACA for 12 hours, either alone or in combination with Z-VAD-FMK (a pan-caspase inhibitor), DEVD-FMK (a caspase 3 inhibitor), Z-IETD-FMK (a caspase 8 inhibitor), or LEHD-CHO (a caspase 9 inhibitor). ACA-induced apoptosis was almost completely blocked by Z-VAD-FMK and by combination of Z-IETD-FMK and LEHD-FMK, although Z-IETD-FMK or LEHD-FMK alone partially inhibited ACA-induced apoptosis in RPMI8226 cells (Fig. 2*B*). In addition, the preincubation of Z-VAD-FMK inhibited the ACA-induced apoptosis of myeloma cells by means of DNA ladder formation analysis (Fig. 1*E*). These results suggest that through treatment with ACA, both of the cascades to the caspase 8 and caspase 9 pathways are activated.

1′-Acetoxychavicol acetate inhibits IκBα phosphorylation and nuclear factor κB activation in myeloma cells. ACA significantly inhibited the serine phosphorylation and degradation of IκBα in a time-dependent manner (Fig. 2*C*). Because the phosphorylation of IκB has been shown to be the primary

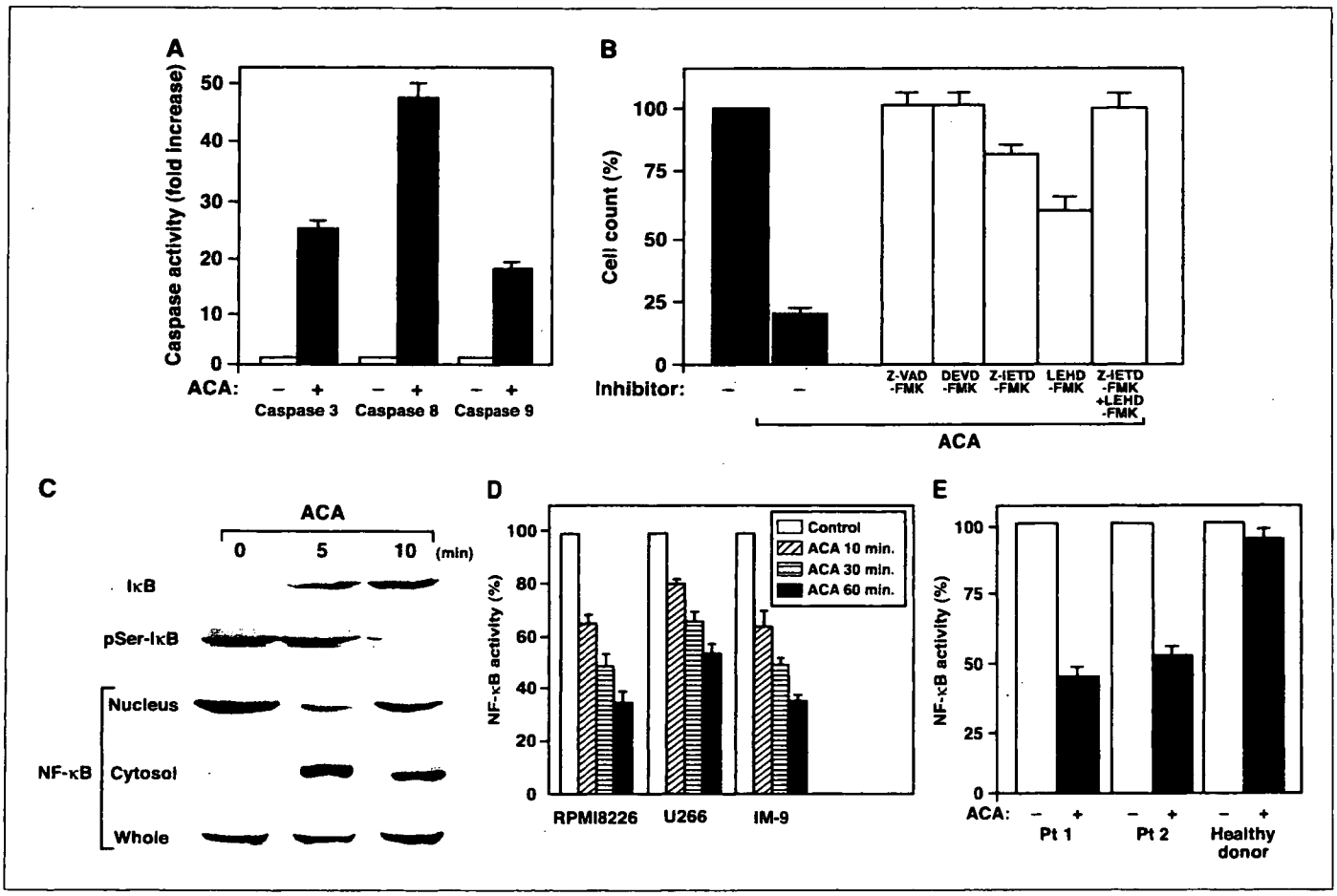

Figure 2. Effects of ACA on caspase and NF-κB activation. *A*, RPMI8226 cells were incubated with 10 μmol/L ACA for 3 hours and then analyzed for activation of caspase 3, 8, and 9 by flow cytometry and colorimetric assay. Each caspase activity in the ACA-treated cells was presented as a fold increase of the control cells. *B*, inhibition of ACA-induced apoptosis in RPMI8226 cells was estimated in a preincubation of Z-VAD-FMK. The cells were preincubated with 20 μmol/L Z-VAD-FMK for 1 hour before the addition of 10 μmol/L ACA. The cell counts were evaluated after 6 hours of incubation. Then, effects of specific caspase inhibitors on ACA-induced apoptosis were examined. The cells were preincubated with each caspase inhibitor [50 μmol/L DEVD-FMK (a caspase 3 inhibitor), 50 μmol/L Z-IETD-FMK (a caspase 8 inhibitor), and 50 μmol/L LEHD-FMK (a caspase 9 inhibitor)] for 1 hour, and then incubated with 10 μmol/L ACA for 6 hours. Cell viability was assessed by trypan blue dye exclusion. *Columns*, mean of three separate experiments done in triplicate; *bars*, SD. *C*, effects of ACA on IκBα phosphorylation and the constitutive expression of NF-κB in myeloma cells. RPMI8226 cells were treated with ACA (10 μmol/L) for the indicated times. Cell lysates (15 μg of protein per lane) were fractionated on 12.5% SDS-polyacrylamide gels and analyzed by Western blotting with antibodies against IκBα and pSer32-IκBα. Nuclear and cytoplasmic extracts and whole cell lysates were prepared to check the level of NF-κB by Western blotting. *D*, ACA down-regulates constitutive NF-κB activity in myeloma cells in a time-dependent manner. The DNA binding activity of transcriptional factor NF-κB was quantified in myeloma cells (RPMI8226, U266, and IM-9) pretreated with 10 μmol/L ACA for the indicated times. The DNA binding activity of NF-κB in the myeloma cells was quantified by ELISA with the use of the Trans-AM NF-κB p65 Transcription Factor Assay Kit, according to the instruction of the manufacturer. Values (mean ± SD) were normalized for the cellular protein contents. *E*, ACA decreased the constitutive NF-κB activity in freshly isolated myeloma cells from two patients, but not in bone marrow mononuclear cells from a healthy donor.

mechanism of NF-κB activation, we next examined whether ACA-induced apoptosis is a result of the inhibition of NF-κB activation. ACA rapidly induced a strong decrease in the NF-κB expression in the nucleus, whereas the protein accumulated in the cytosol in RPMI8226 cells, indicating that ACA inhibited the translocation of NF-κB from the cytosol to the nucleus (Fig. 2*C*). We also confirmed the inhibitory effects of ACA on NF-κB activation by ELISA in several myeloma cell lines, as well as in primary samples from patients with multiple myeloma, but not in normal cells (Fig. 2*D* and *E*; Table 1).

1′-Acetoxychavicol acetate induced the Fas expression and down-regulation of antiapoptotic proteins in RPMI8226 cells. ACA rapidly activated caspase 8, and its specific inhibitor partially inhibited ACA-induced apoptosis in RPMI8226 cells (Fig. 2*A*). Therefore, we investigated whether or not the Fas-mediated pathway was involved in the ACA-induced apoptosis. The suppression of Fas by an antagonistic anti-Fas antibody (ZB4) dramatically inhibited ACA-induced apoptosis (Fig. 3*A*). Consistent with these results, the expression of Fas on the plasma membrane was significantly increased immediately after treatment with ACA with the induction of the Fas ligand (FasL; Fig. 3*B* and data not shown). ACA also rapidly induced the recruitment of caspase 8 to Fas-associated death domain–containing protein, suggesting that ACA induced the formation of death-inducing signaling complex (data not shown). These results indicate that the apoptotic pathway related to Fas/FasL also seems to be involved in ACA-induced apoptosis. Several studies revealed that RPMI8226 cells were resistant to Fas-mediated apoptosis because of higher levels of expression for various antiapoptotic proteins such as FLIP and XIAP. ACA down-regulated the antiapoptotic proteins FLIP and XIAP, but increased the expression of proapoptotic cytosolic AIF (Fig. 3*B*).

Effects of 1′-acetoxychavicol acetate on tumor necrosis factor α–induced sequelae in myeloma cells. TNF-α is known to activate NF-κB and have a small stimulatory effect on myeloma cell proliferation (25). However, TNF-α triggers death-receptor–mediated apoptosis in myeloma cells treated with the NF-κB inhibitor in association with the down-regulation of expression of cIAP-1. In our study, the stimulatory effect of TNF-α on the NF-κB DNA binding activity was completely inhibited by the treatment with 5 μmol/L ACA (Fig. 4*A*). TNF-α–induced apoptosis in RPMI8226 cells cotreated with a nontoxic concentration of ACA (5 μmol/L) corresponded to NF-κB inactivation (Fig. 4*B*). In addition, the treatment with TNF-α slightly up-regulated the expression of well-known NF-κB target molecules, the FLIP and XIAP proteins (Fig. 4*C*). In contrast, cotreatment with ACA and TNF-α strongly inhibited the induction of these proteins (Fig. 4*C*). In addition, ACA decreased the levels of another NF-κB target gene, the adhesion molecule ICAM, in TNF-α–treated RPMI8226 cells (Fig. 4*C*). These data further suggest that NF-κB is an important molecule for the regulation of myeloma cell adhesion and for the interaction of myeloma cells in the bone marrow microenvironment.

Activation of protein kinase C by phorbol 12-myristate 13-acetate protects cells from 1′-acetoxychavicol acetate–induced apoptosis. PMA is a tumor promoter phorbol ester recognized to be a general activator of protein kinase C (PKC; ref. 26). PMA is also known to be an NF-κB activator mediated by the induction of the nuclear translocation of NF-κB (27). A number of previous studies have reported that the activation of PKC by PMA suppresses death receptor–mediated apoptosis through the activation of NF-κB (28). In our study, pretreatment with PMA dramatically attenuated ACA-induced apoptosis by the treatment with ACA (Fig. 4*D*). In addition, pretreatment with PMA abrogated ACA-mediated caspase 8 activation and NF-κB inactivation in myeloma cells (data not shown). TLCK, a serine protease inhibitor, is known to sensitize Fas-mediated apoptosis, even in cells resistant to Fas-induced apoptosis. Several reports have also shown that TLCK can inhibit NF-κB activity by blocking PKC (29, 30). Low-dose TLCK (5 μmol/L) dramatically enhanced the apoptosis of low-dose ACA (5 μmol/L)–treated RPMI8226 cells with the activation of caspase 8 and NF-κB inactivation (Fig. 4*E*). These results also suggest that the ACA-induced apoptosis was mediated through NF-κB inactivation. In addition, low-dose MG132 (5 μmol/L), an excellent proteasome inhibitor, synergistically enhanced ACA-induced apoptosis with caspase 8 activation and NF-κB inactivation (Fig. 4*F*), strongly supporting that ACA induces the apoptosis of multiple myeloma cells through NF-κB inactivation.

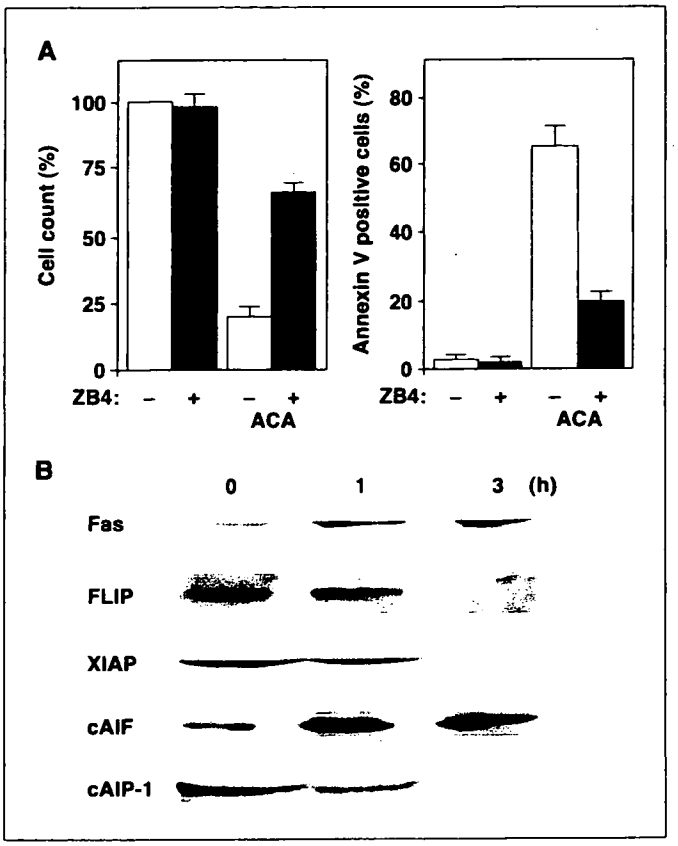

Figure 3. ACA-induced apoptosis in myeloma cells is mediated through the Fas pathway. *A*, antagonistic anti-Fas antibody (ZB4) blocks ACA-induced apoptosis in RPMI8226 cells. RPMI8226 cells were preincubated for 1 hour in the presence of 500 ng/mL of ZB4 antagonistic anti-Fas antibody, and then treated with 10 μmol/L ACA for 12 hours. Cell viability was assessed by trypan blue dye exclusion (*left*), and apoptotic cell death was analyzed by annexin V staining (*right*). *Columns*, mean of three independent experiments; *bars*, SD. *B*, expression of Fas-related proteins in ACA-treated RPMI8226 cells. The cells were treated with 10 μmol/L ACA for the indicated times. Cell lysates (15 μg of protein per lane) were fractionated on 12.5% SDS-polyacrylamide gels and analyzed by Western blotting with antibodies against Fas, FLIP, XIAP, cytosolic AIF (cAIF), and cIAP-1. Reblotting with β-actin staining showed that equal amounts of protein were presented in each lane (data not shown).

Effects of 1′-acetoxychavicol acetate *in vivo*. Our *in vitro* data prompted us to examine whether the effects of ACA are equally valid *in vivo*. Tumor weight decreased in the mice that were injected with ACA (mean weight: 0.04 ± 0.06 g in the ACA-treated group versus 0.63 ± 0.29 g in the control group; Fig. 5*A* and *B*). During treatment,

the ACA-treated mice appeared healthy. In addition, pathologic analysis at autopsy revealed no ACA-induced tissue changes in any of the organs. These results suggest that ACA had no toxic effects on the mice throughout the treatment.

Discussion

In this study, we showed for the first time that ACA, a traditional Asian condiment, induces the apoptosis of human multiple myeloma cell lines as well as of freshly obtained samples from patients with multiple myeloma through inhibition of NF-κB activity. Furthermore, ACA exhibited *in vivo* antimyeloma activity in NOD/SCID mice with no side effects. In addition, ACA did not affect the cellular growth of bone marrow cells from healthy volunteers.

Multiple myeloma is an incurable hematologic malignancy of plasma cells, despite advances in conventional chemotherapy or high-dose chemotherapy with stem cell transplantation (7–9). Therefore, novel therapeutic approaches are urgently needed in clinical settings. The recent understanding that has been gained into the biology of myeloma has led to the development of biological treatments, such as thalidomide and bortezomib, which target the myeloma cells and the bone marrow microenvironment (8, 31). In early clinical trials, these agents have shown remarkable activities against refractory multiple myeloma, but prolonged drug exposure may result in the development of *de novo* drug resistance (32, 33). Therefore, the identification and validation of additional novel targeted therapies for patients with multiple myeloma are needed. The transcription factor NF-κB has been identified as a critical component of several signal transduction pathways (34). NF-κB is an important transcription factor because of its ability to protect cells from apoptosis (35–37). Consequently, NF-κB has

Figure 4. Effects of ACA on TNF-α–induced NF-κB activity and its sequelae in myeloma cells. RPMI8226 cells were treated with 50 ng/mL TNF-α for 12 hours, and then the cells were incubated with a nontoxic dose (5 μmol/L) of ACA for 3 hours. *A*, the DNA binding activity of NF-κB in the myeloma cells was quantified by ELISA with the use of the Trans-AM NF-κB p65 Transcription Factor Assay Kit. A nontoxic dose of ACA significantly inhibited the stimulatory effect of TNF-α on the NF-κB DNA binding activity ($P < 0.001$). *B*, the induction of apoptosis was examined by annexin V/PI double staining. Representative of three duplicate experiments. *C*, ACA inhibited the TNF-α–induced FLIP, XIAP, and ICAM-1 expressions on myeloma cells. RPMI8226 cells were incubated with 10 μmol/L ACA with or without 50 ng/mL TNF-α for 12 hours, and then cell lysates (15 μg of protein per lane) were fractionated on 12.5% SDS-polyacrylamide gels and analyzed by Western blotting. *D*, RPMI8226 cells were treated with 20 μg/mL PMA for 1 hour, and the cells were then incubated with 10 μmol/L ACA for 6 hours. Induction of apoptosis was examined by annexin V/PI double staining. *E*, RPMI8226 cells were treated with a nontoxic dose (5 μmol/L) of ACA and/or low-dose TLCL (5 μmol/L) for 24 hours. The assays for the caspase 8 activity (*left*) were analyzed by flow cytometry analysis, and the NF-κB activity (*right*) was evaluated by ELISA. *Columns*, mean of three separate experiments done in triplicate; *bars*, SD. *F*, RPMI8226 cells were treated with a nontoxic dose (5 μmol/L) of ACA with low dose (5 μmol/L) of MG132 for 24 hours. Neither agent alone in this concentration affected the cellular growth of RPMI8226 cells. The assays for the caspase 8 activity (*left*) were analyzed by flow cytometry analysis, and the NF-κB activity (*right*) was evaluated by ELISA. *Columns*, mean of three separate experiments done in triplicate; *bars*, SD.

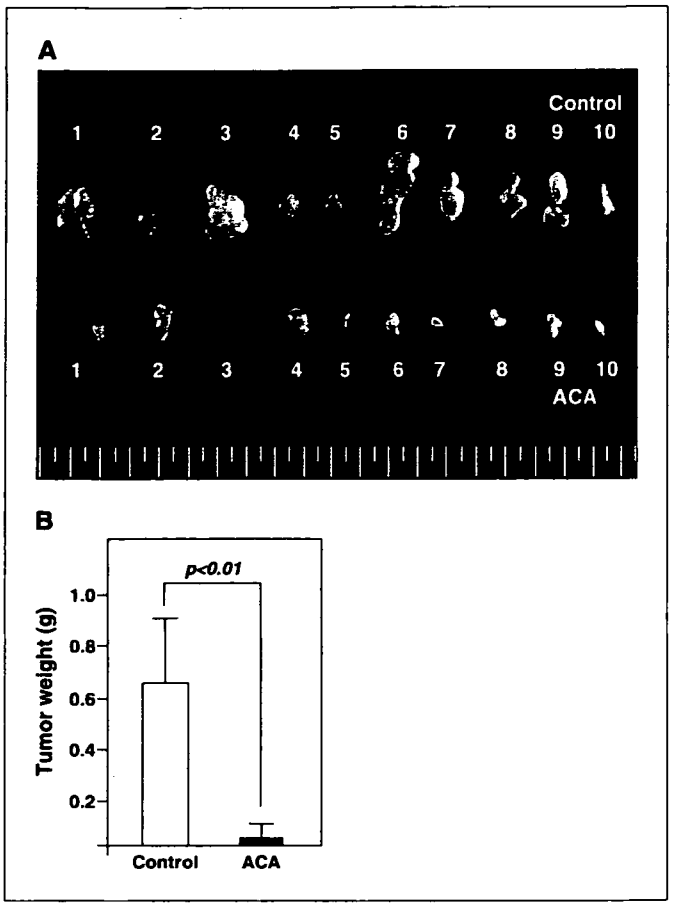

Figure 5. ACA-induced apoptosis of myeloma cells *in vivo* using NOD/SCID mice model. RPMI8226 cells (1×10^7) were inoculated s.c. into NOD/SCID mice. Seven days after transplantation, PBS (control; $n = 10$) or ACA (3 mg/kg; $n = 10$) was given i.p. once every 3 days for 2 weeks. After 2 weeks of treatment, the mice were sacrificed, and the tumor weights measured. *A*, tumors in both the control (*upper*) and ACA-treated (*lower*) mice at autopsy. *B*, ACA significantly decreased the tumor weights in the ACA-treated mice compared with the controls ($P < 0.001$).

emerged as a therapeutic target in a variety of neoplasias, and the NF-κB inhibitor induces apoptosis in myeloma cells (37). In the present study, we investigated the effects of ACA on NF-κB activity in myeloma cells *in vitro* and *in vivo*, and found for the first time that ACA inhibited NF-κB activity in multiple myeloma cell lines and patient cells, but not in normal cells. ACA also sensitized myeloma cells to TNF-α and had a synergistic proapoptotic effect with NF-κB inhibitors, MG-132 and TLCK. In contrast, an excellent NF-κB activator, PMA, dramatically abrogated ACA-induced apoptosis. These results provide the framework for targeting NF-κB inhibition by treatment with ACA in multiple myeloma therapy.

RPMI8226, U266, and IM-9 cells used in this study were relatively resistant to the NF-κB inhibitors (38) because these cells constitutively expressed higher levels of various antiapoptotic molecules including FLIP, cIAP-1, XIAP, and survivin. ACA decreased the levels of these proteins in myeloma cells. The inhibition of NF-κB stimulates caspase 9–dependent apoptosis through the reduction of XIAP and caspase 8–dependent apoptosis mediated through the decrease in FLIP. In our study, ACA activated both cascades to the caspase 8 and caspase 9 pathways in association with NF-κB inactivation, suggesting that ACA has a strong potential for inhibiting the proliferation of myeloma cells through various apoptotic signaling pathways.

The induction of NF-κB with the related up-regulation of adhesion molecules, including CD54 (ICAM-1) and CD106 (VCAM-1), has been shown in TNF-α–stimulated myeloma cell lines and bone marrow stromal cells (25, 39). In addition, myeloma cell adhesion to fibronectin mediates an antiapoptotic effect against chemotherapeutic agents (40, 41). In this study, ACA inhibited the TNF-α–induced up-regulation of the adhesion molecule ICAM-1 expression in RPMI8226 cells, suggesting that ACA may also modulate myeloma cell adhesion to stromal cells in the bone marrow. Several studies have revealed that the inhibition of NF-κB abrogates the induction of IL-6 secretion in bone marrow stromal cells and the proliferation of adherent myeloma cells (25, 39). The ACA-mediated inhibition of adhesion molecule expression, the abrogation of protection against apoptosis conferred by myeloma cells by binding to bone marrow stromal cells, and the blockade of cytokine secretion in the bone marrow milieu provide a further rationale for targeting NF-κB in novel therapies for multiple myeloma.

Finally, ACA had a synergistic proapoptotic effect with the NF-κB inhibitors MG132 and TLCK, and the NF-κB activator PMA inhibited ACA-induced apoptosis, suggesting that ACA induced apoptosis through the inhibition of NF-κB activity. The blockade of NF-κB signaling may represent a novel therapeutic strategy in multiple myeloma (7–9, 31, 32). Because NF-κB activity mediates survival and drug resistance in myeloma cells, the down-regulation of its activity by ACA, as recently observed with proteasome inhibitors (20), could also contribute to its antimyeloma activity. Our finding that ACA down-regulates the constitutive activity of NF-κB in myeloma cells further suggests that it may have combined antimyeloma activity with conventional or novel therapies that also target NF-κB.

In clinical settings, the therapeutic approach to multiple myeloma is basically chemotherapy, but severe side effects, complications, and resistance are major problems. In particular, the side effects of anticancer drugs can be fatal in elderly patients or immunocompromised patients. ACA, which is a component of a traditional Thai condiment, is a natural compound which seems to be safer than current chemotherapeutic drugs. ACA remarkably inhibited the cellular growth of myeloma cells from patients by the induction of apoptosis, whereas the same dose of ACA did not affect the cellular growth of cells from healthy volunteers, indicating that the effects of ACA are specific to malignant cells. We also showed the anticancer effects of ACA *in vivo* with no toxic effects. The Fas receptor is constitutively expressed in the liver; therefore, the liver might be very sensitive to Fas-induced apoptosis, and mice treated with an agonistic anti-CD95 antibody died from hepatic failure caused by the generalized apoptosis of hepatocytes (42). However, we could not observe any organ damage *in vivo* in our study. These results strongly indicate that it might be possible to develop ACA as a new potent anticancer agent for the management of multiple myeloma and as a novel therapeutic agent that can replace the more cytotoxic agents currently used to treat patients with multiple myeloma.

Acknowledgments

Received 1/13/2005; accepted 3/8/2005.

Grant support: Ministry of Education, Culture, Sports, Science and Technology of Japan (M. Kizaki), and a grant from the Mitsubishi Pharma Research Foundation (M. Kizaki).

The costs of publication of this article were defrayed in part by the payment of page charges. This article must therefore be hereby marked *advertisement* in accordance with 18 U.S.C. Section 1734 solely to indicate this fact.

We thank Kaori Saito for her excellent technical assistance.

References

1. Kondo A, Ohigashi H, Murakami A, Jiwajinda S, Koshimizu K. A potent inhibitor of tumor promoter-induced Epstein-Barr virus activation, 1′-acetoxychavicol acetate from Languas galanga, a traditional Thai condiment. Biosci Biotechnol Biochem 1993;57: 1344–5.
2. Ohnishi M, Tanaka T, Makita H, et al. Chemopreventive effect of a xanthine oxidase inhibitor, 1′-acetoxychavicol acetate, on rat oral carcinogenesis. Jpn J Cancer Res 1996;87:349–56.
3. Moffatt J, Hashimoto M, Kojima A, et al. Apoptosis induced by 1′-acetoxychavicol acetate in Ehrlich ascites tumor cells is associated with modulation of polyamine metabolism and caspase-3 activation. Carcinogenesis 2000;21:2151–7.
4. Nakamura Y, Murakami A, Ohto Y, Torikai K, Tanaka T, Ohigashi H. Suppression of tumor promoter-induced oxidative stress and inflammatory responses in mouse skin by a superoxide generation inhibitor 1′-acetoxychavicol acetate. Cancer Res 1998;58:4832–9.
5. Tanaka T, Makita H, Kawamori T, et al. A xanthine oxidase inhibitor 1′-acetoxychavicol acetate inhibits azoxymethane-induced colonic aberrant crypt foci in rats. Carcinogenesis 1997;18:1113–8.
6. Ito K, Nakazato T, Murakami A, et al. Induction of apoptosis in human myeloid leukemic cells by 1′-acetoxychavicol acetate through a mitochondrial- and Fas-mediated dual mechanism. Clin Cancer Res 2004; 10:2120–30.
7. Hideshima T, Anderson KC. Molecular mechanisms of novel therapeutic approaches for multiple myeloma. Nat Rev Cancer 2002;2:927–37.
8. Sirohi B, Powles R. Multiple myeloma. Lancet 2004;363:875–87.
9. Hideshima T, Bergsagel PL, Kuehl WM, Anderson KC. Advances in biology of multiple myeloma: clinical applications. Blood 2004;104:607–18.
10. Bendall HH, Sikes ML, Ballard DW, Oltz EM. An intact NF-κB signaling pathway is required for maintenance of mature B cell subsets. Mol Immunol 1999; 36:187–95.
11. Doerre S, Corley RB. Constitutive nuclear transcription of NF-κB in B cells in the absence of IκB degradation. J Immunol 1999;169:269–77.
12. Baldwin AS Jr. The NF-κB and IκB proteins: new discoveries and insights. Annu Rev Immunol 1996;14: 649–81.
13. Ghosh S, May MJ, Kopp EB. NF-κB and Rel proteins: evolutionarily conserved mediators of immune responses. Annu Rev Immunol 1998;16:225–60.
14. DiDonato JA, Mercurio F, Karin M. Phosphorylation of IκBα precedes but is not sufficient for its dissociation from NF-κB. Mol Cell Biol 1995;15:1302–11.
15. Feinman R, Koury J, Thames M, Barlogie B, Epstein J, Siegel DS. Role of NF-κB in the rescue of multiple myeloma cells from glucocorticoid-induced apoptosis by bcl-2. Blood 1999;93:3044–52.
16. Ni H, Ergin M, Huang Q, et al. Analysis of expression of nuclear factor κB (NF-κB) in multiple myelom: down-regulation of NF-κB induces apoptosis. Br J Haematol 2001;115:279–86.
17. Chauhan D, Uchiyama H, Akbarali Y, et al. Multiple myeloma cell adhesion-induced interleukin-6 expression in bone marrow stromal cells involves activation of NF-κB. Blood 1996;87:1104–12.
18. Keifer JA, Guttridge DC, Ashburner BP, Baldwin AS Jr. Inhinbition of NF-κB activity by thalidomide through suppression of IκB kinase activity. J Biol Chem 2001;276: 22382–7.
19. Palombella VJ, Conner EM, Fuseler JW, et al. Role of the proteasome and NF-κB in streptococcal cell wall-induced polyarthritis. Proc Natl Acad Sci U S A 1998;95: 15671–6.
20. Hideshima T, Richardson P, Chauhan D, et al. The proteasome inhibitor PS-341 inhibits growth, induces apoptosis, and overcomes drug resistance in human multiple myeloma. Cancer Res 2001;61:3071–6.
21. Hideshima T, Chauhan D, Richardson P, et al. NF-κB as a therapeutic target in multiple myeloma. J Biol Chem 2002;277:16639–47.
22. Murakami A, Toyota K, Okura S, Koshimizu K, Ohigasgi H. Structure-activity relationships of (1′*S*)-1′-acetoxychavichol acetate, a major constituent of a Southeast Asia condiment plant Langus galangal, on the inhibition of tumor-promoter-induced Epstein-Barr virus activation. J Agric Food Chem 2000;48: 1518–23.
23. Ito K, Nakazato T, Yamato K, et al. Induction of apoptosis in leukemic cells by homovanillic acid derivative, capsaicin, through oxidative stress: implication of phosphorylation of p53 at Ser-15 residue by reactive oxygen species. Cancer Res 2004;64:1071–8.
24. Workman P, Balman A, Hickman JA, et al. UKCCCR guidelines for the welfare of animals in experimental neoplasia. Br J Cancer 1998;58:109–13.
25. Hideshima T, Chauhan D, Schlossman R, Richardson P, Anderson KC. The role of tumor necrosis factor α in the pathophysiology of human multiple myeloma: therapeutic applications. Oncogene 2001;20:4519–27.
26. Kvanta A, Jondal M, Fredholm BB. Translocation of the α- and β-isoforms of protein kinase C following activation of human T-lymphocytes. FEBS Lett 1991;283: 321–4.
27. Epinat JC, Gilmore TD. Diverse agents act at multiple levels to inhibit the Rel/NF-κB signal transduction pathway. Oncogene 1999;18:6896–909.
28. Meng XW, Heldebrant MP, Kaufman SH. Phorbol 12-myristate 13-acetate inhibits death receptor-mediated apoptosis in Jurkat cells by disrupting recruitment of Fas-associated polypeptide with death domain. J Biol Chem 2002;277:3776–83.
29. Lee Y, Shacter E. Fas aggregation does not correlate with Fas-mediated apoptosis. J Immunol 2001;167:82–9.
30. Solomon DH, O'Brian CA, Weinstein IB. *N*-α-Tosyl-L-lysine chloromethyl ketone and *N*-α-tosyl-L-phenylalanine chloromethyl ketone inhibit protein kinase C. FEBS Lett 1985;190:342–4.
31. Bruno B, Rotta M, Giaccone L, et al. New drugs for treatment of multiple myeloma. Lancet Oncol 2004;5: 430–42.
32. Hideshima T, Richardson P, Anderson KC. Novel therapeutic approaches for multiple myeloma. Immunol Rev 2003;194:164–76.
33. Bartlett JB, Dredge K, Dalgleish AG. The evolution of thalidomide and its IMiD derivatives as anticancer agents. Nat Rev 2004;4:314–22.
34. Barnes. PJ, Karin M. Nuclear factor-κB: a pivotal transcription factor in chronic inflammatory diseases. N Engl J Med 1997;336:1066–71.
35. Wang CY, Mayo MW, Baldwin AS Jr. TNF- and cancer therapy-induced apoptosis: potentiation by inhibition of NF-κB. Science 1996;274:784–7.
36. Van Antwerp DJ, Martin SJ, Kafri T, Green DR, Verma IM. Suppression of TNF-α-induced apoptosis by NF-κB. Science 1996;274:787–9.
37. Beg AA, Ruben SM, Scheinman RI, Haskill S, Rosen CA, Baldwin AS Jr. IκB interacts with the nuclear localization sequences of the subunits of NF-κB: a mechanism for cytoplasmic retention. Genes Dev 1992; 6:1899–913.
38. Bharti A, Donato N, Singh S, Aggarwal BB. Curcumin (diferuloylmethane) down-regulates the constitutive activation of nuclear factor-κB and IκBα kinase in human multiple myeloma cells, leading to suppression of proliferation and induction of apoptosis. Blood 2003; 101:1053–62.
39. Hideshima T, Chauhan D, Podar K, Schlossman R, Richardson P, Anderson KC. Novel therapies targeting the myeloma cell and its bone marrow microenvironment. Semin Oncol 2001;28:607–12.
40. Nov H, Holt RU, Rø TB, et al. A selective c-Met inhibitor blocks an autocrine Hepatocyte Growth Factor loop in ANBL-6 cells and prevents migration and adhesion of myeloma cells. Clin Cancer Res 2004;10: 6686–94.
41. Dai Y, Pei X-Y, Rahmani M, Conrad DH, Dent P, Grant S. Interuption of the NF-κB pathway by Bay 11-7082 promotes UCN-01-mediated mitochondrial dysfunction and apoptosis in human multiple myeloma cells. Blood 2004;103:2761–70.
42. Kondo T, Suda T, Fukuyama H, Adachi M, Nagata S. Essential role of the Fas ligand in the development of hepatitis. Nat Med 1997;3:409–13.

J Bone Miner Metab (2005) 23:270–273
DOI 10.1007/s00774-004-0595-y

SHORT COMMUNICATION

**Ryoji Fujimaki · Katsuhiko Hayashi · Naoko Watanabe
Taketo Yamada · Yoshiaki Toyama · Ken-ichi Tezuka
Nobumichi Hozumi**

Expression of Cre recombinase in the mouse developing chondrocytes driven by the mouse α2(XI) collagen promoter

Received: June 14, 2004 / Accepted: October 26, 2004

Key words Cre-LoxP · Chondrocyte · α2(XI) collagen gene

Introduction

Endochondral bone formation is a highly coordinated process of skeletal development, through which all the longitudinal bones are created. Endochondral bone formation is initiated with the condensation of mesenchymal cells. Then, aggregated mesenchymal cells subsequently differentiate into cartilage, and later primordial cartilages are replaced by bone. Thus, considering the fact that chondrogenesis precedes bone formation in endochondral bone formation, investigation of chondrogenesis provides the key to understanding the molecular mechanisms involved in skeletogenesis.

Targeted gene deletion (gene knockout) technology is versatile in the fields of skeletal biology. However, the conventional gene knockout approach sometimes leads to embryonic lethality before bone formation, and the problem makes it difficult to elucidate the function of genes. The Cre-loxP system was established to overcome this limitation. The Cre-loxP system enables us to design experiments to disrupt genes in a time- and site-specific manner, and it is becoming a powerful tool for analyzing gene function in vivo. This system is based on the principle that the bacteriophage P1 Cre recombinase recognizes the specific sequences, called loxP sites, and excises the DNA floxed by the two loxP sites. Two mouse lines are required for the conditional gene deletion experiment: a mouse strain carrying a target gene flanked by two loxP sites, and a conventional transgenic mouse strain expressing Cre recombinase under the control of a transgenic promoter. Mating of these two mouse lines results in Cre-mediated gene disruption only within the cells in which the promoter is activated, and Cre recombinase is expressed.

Type XI collagen, which is one of the structural components of the cartilage matrix, is constituted by three distinct subunits: α1(XI), α2(XI), and α3(XI). Type XI collagen plays a critical role in regulating the formation of the collagen fibrils. Chondrodysplasia in *cho/cho* mice is caused by a mutation in the α1(XI) gene [1]. It has been also reported that mutations in the α2(XI) gene cause chondrodysplasias in humans, such as Stickler syndrome [2]. Although the α1(XI) and α3(XI) genes are expressed in many tissues other than cartilage, expression of the mouse α2(XI) gene is more restricted to cartilage [3–5], and the 5′-flanking region of the α2(XI) collagen gene has been documented by Tsumaki et al. [6]. They demonstrated that the upstream 742-bp sequence of the transcriptional start site of the α2(XI) collagen gene contained genetic elements required for specific expression in cartilage.

We generated Cre-expressing transgenic mice under the control of the −742-bp promoter sequence of the mouse α2(XI) collagen gene. In this article, we report the establishment of a mouse line that expresses Cre recombinase driven by the α2(XI) collagen promoter and show this mouse line will be a useful tool for analyzing the role of various genes involved in the complicated process of chondrogenesis.

R. Fujimaki · N. Watanabe · N. Hozumi (✉)
Research Institute for Biological Sciences, Tokyo University of Science (RIKADAI), 2669 Yamazaki, Noda 278-0022, Japan
Tel. +81-4-7121-4091; Fax +81-4-7121-4099
e-mail: nobhozmi@rs.noda.tus.ac.jp

K. Hayashi
Department of Molecular Embryology Research Institute, Osaka Medical Center for Maternal and Child Health, Osaka, Japan

T. Yamada
Department of Pathology, Keio University School of Medicine, Tokyo, Japan

R. Fujimaki · Y. Toyama
Department of Orthopaedic Surgery, Keio University School of Medicine, Tokyo, Japan

K. Tezuka
Department of Tissue and Organ Development, Gifu University Graduate School of Medicine, Gifu, Japan

Materials and methods

DNA construction and production of transgenic mice

The transgenic construct was generated from Pnass-lacZ-Int (gift from Dr. N. Tsumaki) [6], which carries the −742-bp promoter sequence of the mouse α2(XI) collagen gene, SV40 RNA splice site, β-galactosidase gene, SV40 polyadenylation signal, and the first intron of the mouse α2(XI) collagen gene. The β-galactosidase gene was replaced with the Cre gene. The 4.1-kb construct was linearized and microinjected into pronuclei of fertilized BDF1(C57BL/6xDBA2) zygotes according to standard procedures [7].

Polymerase chain reaction analysis and Southern blots

The transgenes were identified by polymerase chain reaction (PCR) and Southern blots on tail and placenta genomic DNA. For PCR analysis, the primers used for Cre gene were Cre-5′, 5′-CCTGGAAAATGCTTCTGTCCGTTT GCC-3′; Cre-3′, 5′-GAGTTGATAGCTGGCTGGTGG CAGATG-3′, as described [8]. For Southern blot analysis, tail DNA were digested with *Xho*I, fractionated on 0.8% agarose gel, transferred to a nylon membrane (Hybond-N; Amersham-Pharmacia Biotech, Tokyo, Japan) and probed with an 0.6-kb, digoxigenin (DIG)-labeled PCR fragment of Cre gene.

X-gal staining and histology

Embyos and neonates were fixed with 2% paraformaldehyde and 0.2% glutaraldehyde for 1 h at 4°C, washed three times with phosphate-buffered saline (PBS), and incubated in staining solutions [1 mg/ml 5-bromo-4-chloro-3-indolyl β-D-galactopyranoside (X-gal), 4 mM $K_4Fe(CN)_6$, 4 mM $K_3Fe(CN)_6$, 2 mM $MgCl_2$ in PBS] at 37°C overnight. Specimens were embedded in wax, sectioned, and counterstained with eosin or kernechtrot.

Results and discussion

The Cre recombinase gene was placed downstream of the −742-bp promoter sequence of the mouse α2(XI) collagen gene. The first intron of the α2(XI) collagen gene was placed at the 3′-end of the Cre gene, which is also responsible for cartilage-specific expression (Fig. 1A). Transgene integration in the mouse genome was assessed by genomic PCR and Southern blot using tail DNA extracts (Fig. 1B,C). Five different founder lines were obtained.

These five transgenic mouse lines were crossed with another transgenic mouse line, CAG-CAT-Z, carrying a reporter gene constructed to examine whether the founder lines express sufficiently high Cre recombinase to mediate recombination at loxP sites and reveal the spatiotemporal expression patterns of the gene. The CAG-CAT-Z mouse

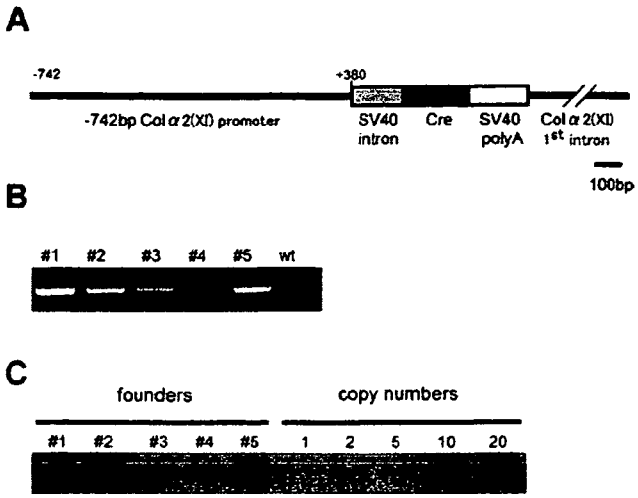

Fig. 1. **A** Schematic diagram of the DNA construct. The Cre recombinase gene was placed under the control of the −742 bp promoter sequence and the first intron of the mouse α2(XI) collagen gene. **B** Founder lines are genotyped by polymerase chain reaction (PCR) using Cre-specific primers. **C** Determination of the copy numbers of founders by quantitative Southern blot

directs expression of the LacZ gene upon Cre-mediated recombination of the loxP-flanked chloramphenicol acetyltransferase (CAT) gene located between the CAG promoter and the lacZ gene [9]. Embryos were stained with X-gal to detect β-gal activity.

Founder line #2 showed Cre activity in chondrocytes, parts of the brain, and neural tubes (data not shown). The −518-bp and −530-bp promoter sequences of the α2(XI) collagen gene direct artificial expression in neural tissues [10]. We speculated that the promoter region of the transgene in founder line #2 was partially shortened physically or functionally during transgene integration and directed expression of Cre in neural tissues. Founder line #3 showed Cre activity in the whole body. This expression pattern, which cannot be explained by the previous studies [6,10], might be due to position effects at the site of transgene integration in the genome. Founder lines #1 and #5 failed to demonstrate Cre recombinase activity.

Founder line #4 revealed a desirable result for our purpose, although copy numbers of the transgene were the smallest among the five founder lines (Fig. 1C). Embryos (founder line #4 × CAG-CAT-Z F1) showed weak β-gal activity in the notochord at 11.0 days postcoitum (dpc) (Fig. 2A). By 12.5 dpc, lacZ expression was evident in primordial cartilages of forelimb and notochord remnant (Fig. 2B). Histological sections of the radius and ulna revealed that LacZ was uniformly expressed in every chondrocyte of primordial cartilages (Fig. 2C). Cre has not yet been expressed in mesenchymal condensation areas of the forefoot plate, which are supposed to become chondrocytes in later stages (Fig. 2D). By 14.5 dpc, β-gal activity was observed in the endochondral bone formation areas such as forelimbs and hindlimbs, ribs, scapula, and vertebrae (Fig. 2E). No lacZ staining was visible in any tissues other than cartilages. In the 2-day-old neonate, lacZ staining was also visible in other

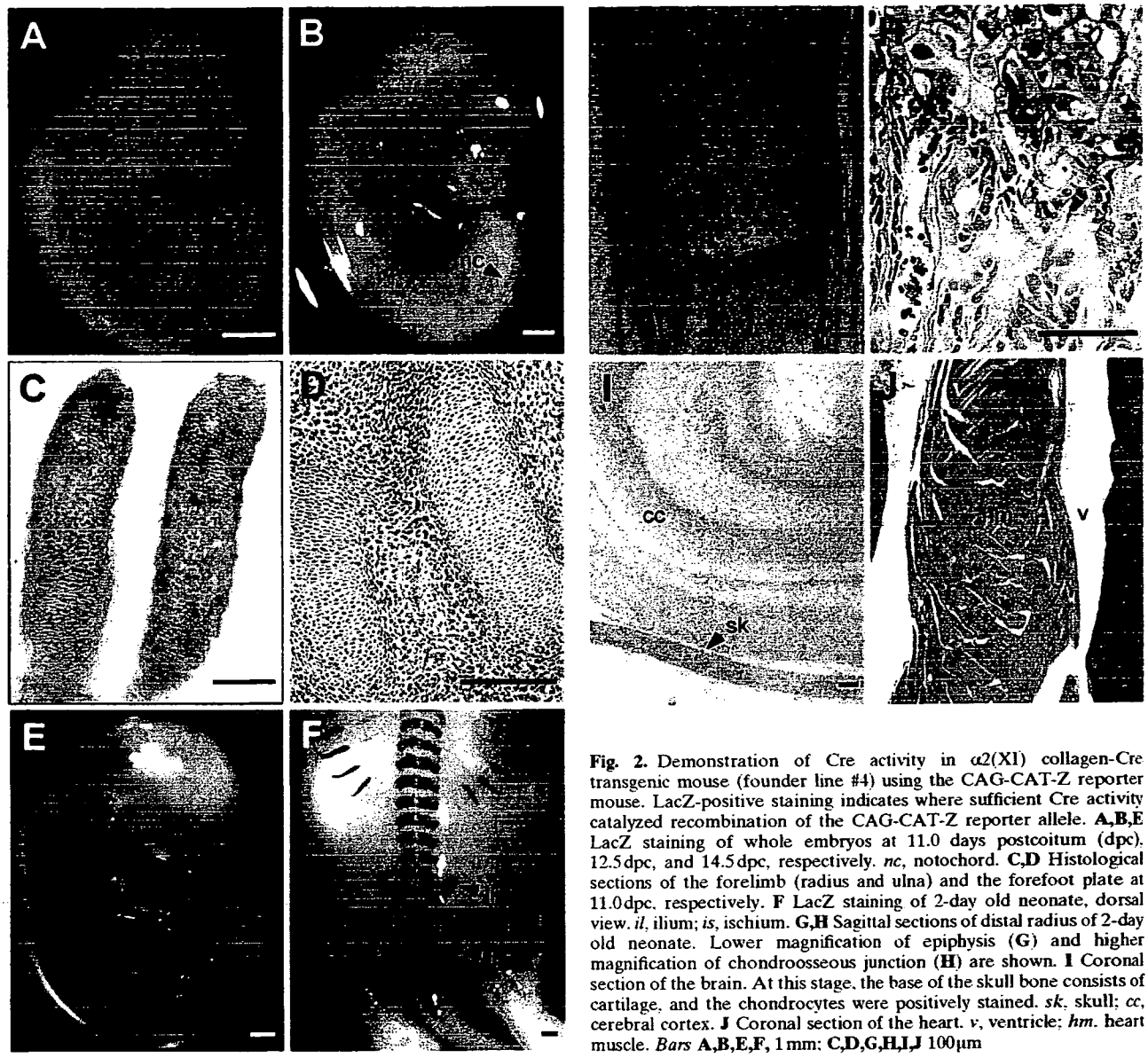

Fig. 2. Demonstration of Cre activity in α2(XI) collagen-Cre transgenic mouse (founder line #4) using the CAG-CAT-Z reporter mouse. LacZ-positive staining indicates where sufficient Cre activity catalyzed recombination of the CAG-CAT-Z reporter allele. **A,B,E** LacZ staining of whole embryos at 11.0 days postcoitum (dpc), 12.5 dpc, and 14.5 dpc, respectively. *nc*, notochord. **C,D** Histological sections of the forelimb (radius and ulna) and the forefoot plate at 11.0 dpc, respectively. **F** LacZ staining of 2-day old neonate, dorsal view. *il*, ilium; *is*, ischium. **G,H** Sagittal sections of distal radius of 2-day old neonate. Lower magnification of epiphysis (**G**) and higher magnification of chondroosseous junction (**H**) are shown. **I** Coronal section of the brain. At this stage, the base of the skull bone consists of cartilage, and the chondrocytes were positively stained. *sk*, skull; *cc*, cerebral cortex. **J** Coronal section of the heart. *v*, ventricle; *hm*, heart muscle. *Bars* **A,B,E,F,** 1 mm; **C,D,G,H,I,J** 100 μm

endochondral formation areas, such as the ilium, ischium (Fig. 2F) and base of the skull (Fig. 2I). Histological sections of the distal radius of the neonate demonstrated that β-gal activity was observed in all epiphyseal chondrocytes throughout their differentiation stages, from resting to hypertrophic chondrocytes (Fig. 2G). No lacZ staining was detected in the cuboidal osteoblastic cells lining on the cancellous bone (Fig. 1H). We also noted that the #4 transgenic mouse is fertile and viable, implying that the transgene does not disrupt a vital endogenous gene. The activity of the Cre transgene did not change in the offspring mice of founder line #4. This expression pattern of the #4 mouse line was almost identical to that of the previously reported transgenic mouse that directed lacZ expression under the control of the −742-bp promoter [6].

As a chondrocyte-specific Cre-expressing transgenic mouse, the α2(II) collagen promoter directed Cre-expressing mice were previously reported [11,12]. Cre activity was noted in tissues other than cartilage such as heart and osteoblasts, and a small amount of mosaicism in Cre activity was observed in the cartilage. In contrast, we did not detect Cre expression in noncartilage tissues, including heart, brain, and osteoblasts (Fig. 2H–J), except for the notochord, and Cre was uniformly expressed in all chondrocytes we examined. Generally, the expression level of α2(II) collagen is higher than that of α2(XI) collagen, and this may cause more specific Cre recombinase expression in the cartilage of α2(XI)-Cre mice. Therefore, this transgenic mouse line would become an appropriate alternative for the analysis of gene function in chondrogenesis.

Summary

Spatial and temporal gene inactivation by the cre-loxP system is a powerful tool for analyzing genes of interests. We generated a transgenic mouse line that expresses Cre recombinase under the control of the −742-bp promoter sequence of the mouse α2(XI) collagen gene. Crossing this mouse line with a reporter mouse revealed that Cre recombinase activity is observed specifically in developing chondrocytes. This chondrocyte-specific Cre expression was observed from the early stage of chondrocyte differentiation in forelimb at 12.5 dpc, but not expressed in mesenchymal condensations. This transgenic mouse line will be a suitable resource for the analysis of gene function in differentiating chondrocytes and the mechanism of endochondral ossification.

Acknowledgments We thank Dr. Noriyuki Tsumaki for his generous gift for the α2(XI) collagen gene promoter/enhancer construct, Dr. Jun-ichi Miyazaki for providing us with the CAG-CAT-Z, mouse and Dr. Takeshi Miyamoto for technical help. This work was supported in part by grants from the Ministry of Education, Culture, Sports, Science and Technology of Japan.

References

1. Li Y, Lacerda DA, Warman ML, Beir DR, Yoshioka H, Ninomiya Y, Oxford JT, Morris NP, Andrikopoulos K, Ramirez F, Wardell BB, Lifferth GD, Teusher C, Woodward SR, Taylor BA, Seegmiller RE, Olsen BR (1995) A fibrillar collagen gene, Col11a1, is essential for skeletal morphogenesis. Cell 80:423–430
2. Vikkula M, Mariman EC, Lui VC, Zhidkova NI, Tiller GE, Goldring MB, Van Beersum SE, de Waal Malefijt MC, van den Hoogen FH, Ropers HH, Mayne R, Cheah KS, Olsen BR, Warman ML, Brunner HG (1995) Autosomal dominant and recessive osteochondrodysplasias associated with the COL11A2 locus. Cell 80:431–437
3. Yoshioka H, Iyama K, Khaleduzzaman M, Ninomiya Y, Ramirez F (1995) Developmental pattern of expression of the mouse alpha 1 (XI) collagen gene (Col11a1). Dev Dyn 204:41–47
4. Tsumaki N, Kimura T (1995) Differential expression of an acidic domain in the amino-terminal propeptide of mouse pro-alpha 2(XI) collagen by complex alternative splicing. J Biol Chem 270: 2372–2378
5. Sugimoto M, Kimura T, Tsumaki N, Matsui Y, Nakata K, Kawahata H, Yasui N, Kitamura Y, Nomura S, Ochi T (1998) Differential in situ expression of alpha2(XI) collagen mRNA isoforms in the developing mouse. Cell Tissue Res 292:325–332
6. Tsumaki N, Kimura T, Matsui Y, Nakata K, Ochi T (1996) Separable cis-regulatory elements that contribute to tissue- and site-specific α2(XI) collagen gene expression in the embryonic mouse cartilage. J Cell Biol 134:1573–1582
7. Hogan B, Beddington R, Constantini F, Lacy E (1994) Manipulating the Mouse Embryo: A Laboratory Manual, 2nd edn. Cold Spring Harbor Laboratory Press, Cold Spring Harbor, NY
8. Dacquin R, Starbuck M, Schinke T, Karsenty G (2002) Mouse alpha1(I)-collagen promoter is the best known promoter to drive efficient Cre recombinase expression in osteoblast. Dev Dyn 224:245–251
9. Sakai K, Miyazaki J (1997) A transgenic mouse line that retains Cre recombinase activity in mature oocytes irrespective of the cre transgene transmission. Biochem Biophys Res Commun 237:318–324
10. Tsumaki N, Kimura T, Tanaka K, Kimura JH, Ochi T, Yamada Y (1998) Modular arrangement of cartilage- and neural tissue-specific cis-elements in the mouse α2(XI) collagen promoter. J Biol Chem 273:22861–22864
11. Ovchinnikov DA, Deng JM, Ogunrinu G, Behringer RR (2000) Col2a1-directed expression of Cre recombinase in transgenic mice. Genesis 26:145–146
12. Sakai K, Hiripi L, Glumoff V, Brandau O, Eerola R, Vuorio E, Bosze Z, Fassler R, Aszodi A (2001) Stage- and tissue-specific expression of a Col2a1-Cre fusion gene in transgenic mice. Matrix Biol 19:761–767